Title: The immune profile of circulating autoreactive CD4 T cells is imprinted through tissue activation during autoimmune liver diseases

Authors: Anaïs Cardon[1†], Thomas Guinebretière[1†], Chuang Dong[2], Laurine Gil[2], Sakina Ado[2], Pierre-jean Gavlovsky[1], Martin Braud[1], Richard Danger[1], Christoph Schultheiß[3], Aurélie Doméné[4], Perrine Paul-Gilloteaux[4], Caroline Chevalier[5], Laura Bernier[1], Jean-Paul Judor[1], Cynthia Fourgeux[1], Astrid Imbert[6], Marion Khaldi[6, 7], Edouard Bardou-Jacquet[8], Laure Elkrief[9], Adrien Lannes[10], Christine Silvain[11], Matthieu Schnee[12], Florence Tanne[13], Fabienne Vavasseur[5], Lucas Brusselle[1], Sophie Brouard[1], William W Kwok[14], Jean-François Mosnier[1, 15], Ansgar Lohse[16], Jeremie Poschmann[1], Mascha Binder[3], Jérôme Gournay[1, 6, 7], Sophie Conchon[1§], Pierre Milpied[2§*], Amédée Renand[1§*].

[1] Nantes Université, CHU Nantes, INSERM, Center for Research in Transplantation and Translational Immunology, UMR 1064, F-44000 Nantes, France.

[2] Aix Marseille Université, CNRS, INSERM, Centre d'Immunologie de Marseille-Luminy, CIML, Marseille, France.

[3] Laboratory of Translational Immuno-Oncology, Department of Biomedicine, University and University Hospital Basel, Basel, Switzerland.

[4] MicroPICell facility, SFR-Santé, INSERM, CNRS, Nantes Université, CHU Nantes, Nantes, France.

[5] Centre d'Investigation Clinique gastro-nutrition, CHU Nantes, Nantes, France.

[6] Service Hepato-gastro-entérologie et Assistance Nutritionnelle, CHU Nantes, Nantes, France.

[7] Institut des Maladies de l'Appareil Digestif, IMAD, CHU Nantes, Nantes, France.

[8] CHU Rennes, Service des maladies du foie, Université Rennes, INSERM, INRAE, Institut NUMECAN, Rennes, France.

[9] CHRU Tours, Service Hépato-Gastroentérologie, Tours, France.

[10] CHU Angers, Service Hépato-Gastroentérologie et Oncologie Digestive, Université d'Angers, Laboratoire HIFIH, UPRES EA3859, SFR 4208, Angers, France.

[11] CHU Poitiers, Service Hépato-Gastroentérologie, Poitiers, France.

[12] CHD Vendée-La Roche sur Yon, Service Hépato-Gastroentérologie, F- 85000, la Roche sur Yon, France.

[13] CHU Brest, Service Hépato-Gastroentérologie, Brest, France.

[14] Center for Translational Immunology, Benaroya Research Institute, Seattle, WA 98101, USA.

30 [15] Service Anatomie et Cytologie Pathologiques, CHU Nantes, Nantes, France.

31 [16] First Department of Medicine, University Medical Center Hamburg-Eppendorf, Hamburg, Germany.

32 [†] Equal contribution

33 [§] Equal contribution, co-last

34 * Corresponding authors : Dr Amédée Renand, INSERM UMR1064 – Center for Research in
35 Transplantation and Translational Immunology, CHU Nantes – Hôtel Dieu, 30 boulevard Jean Monnet,
36 44093, Nantes Cedex 01, France. Phone: (+33)240087410. E-mail address: amedee.renand@univ-
37 nantes.fr ; Dr Pierre Milpied, INSERM, Centre d'Immunologie de Marseille-Luminy, case 906, Parc
38 scientifique et technologique de Luminy, 13288, Marseille cedex 09, France. Phone : (+33)491269406.
39 E-mail address: milpied@ciml.univ-mrs.fr

40 **Abstract.**

41 Autoimmune liver diseases (AILD) are immune-mediated disorders in which CD4 T cells play a central
42 role. However, the link between circulating self-antigen-specific CD4 T cells and the targeted tissue has
43 not been extensively studied in AILD. We hypothesized that circulating autoreactive CD4 T cells were
44 clonally and functionally related to dominant intra-hepatic pathogenic CD4 T cell clones. Single cell
45 transcriptomic analysis of circulating self-antigen-specific CD4 T cells revealed a specific B-helper and
46 immuno-exhausted transcriptional profile, which was conserved for different autoantigens, but
47 distinct from several other types of foreign antigen specificities. In the blood, the dominant hepatic
48 CD4 T cell clones had a similar transcriptomic signature and were enriched in the PD-1$^+$ TIGIT$^+$ HLA-DR$^+$
49 CD4 T cell subset. In a mouse model, antigen-specific CD4 T cells acquired the immuno-exhausted
50 transcriptional profile when they accumulated in the liver after local antigen reactivity. Locally,
51 immune checkpoint molecules controlled the response of antigen-specific CD4 T cells responsible for
52 liver damage. Our study reveals the origin and biology of liver-derived autoreactive CD4 T cells in the
53 blood of AILD patients that are imprinted by the liver environment, and suggest a dysregulation of the
54 immune checkpoint molecules pathways. Our study enables tracking and isolating circulating
55 autoreactive CD4 T cells for future diagnostic and therapeutic purposes.

56 **Introduction.**

57 Autoimmune liver diseases (AILD) are rare immune-mediated chronic inflammatory diseases. The
58 three main AILD are autoimmune hepatitis (AIH), primary biliary cholangitis (PBC) and primary
59 sclerosing cholangitis (PSC), which are characterized by the destruction of the liver parenchyma, the
60 intrahepatic biliary epithelial cells of small bile ducts or the intra- or extra-hepatic biliary epithelial cells

61 of the large bile ducts, respectively. AIH, PBC and PSC are characterized by immune infiltrates in the
62 liver[1–7]. Autoantibodies are detectable in the serum of patients, especially for AIH and PBC. PSC is a
63 more complex disease often associated with ulcerative colitis[8]. Although all three AILD are classified
64 as autoimmune diseases, the degree of intensity of the autoreactive response appears to be variable,
65 and the link with the autoimmune T-cell signature is unknown. In our study, we focused primarily on
66 AIH and PBC diseases.

67 In AILD, the strong association with the HLA locus, the presence of autoantibodies in serum and T cells
68 in damaged tissue reflects the complete adaptive immune response against self-antigens, with a
69 central role for CD4 T cells with their helper function[9–12]. The recent demonstration of the efficacy of
70 rituximab (anti-CD20) treatment in AIH confirms that B cells contribute to the pathogenesis of AILD[13].
71 However, it has been difficult to establish in-depth the immune profile of autoreactive CD4 T cells, as
72 they are rare in the blood and not all self-antigens are known. During AILD, some target self-antigens
73 have been described. Anti-SLA antibodies target the Sepsecs self-antigen, anti-LKM1 target the CYP2D6
74 self-antigen, anti-LC1 target the FTCD self-antigen and the anti-mitochondrial M2 (anti-M2) antibody
75 target the PDCE2 self-antigen. T cell reactivity against Sepsecs, CYP2D6, FTCD and PDCE2 is detectable
76 in the blood of AILD patients with a preferential Th1 cytokine profile (IFNγ)[14–17]. In a mouse model,
77 immunization against CYP2D6 or FTCD induces liver autoimmunity[18–21]. Those studies reinforce the
78 idea of a complete adaptive immune response against self-antigens in AILD with a central role of CD4
79 T cells. Recently, we were able to characterize the single cell transcriptomic profile of Sepsecs-specific
80 CD4 T cells in the blood of AIH patients with anti-SLA antibodies[22]. Compared to Candida Albicans-
81 specific CD4 T cells, Sepsecs-specific CD4 T cells were PD-1^{+} CXCR5^{-} cells and expressed high level of
82 the B-helper gene, *IL21*, as well as the *IFNG* gene and the immunoregulatory genes *TIGIT* and *CTLA-4,*
83 among others. In the blood of AIH patients, we found an increase in IL21- and IFNγ-producing PD-1^{+}
84 CXCR5^{-} CD4 T cells, independent of the presence of specific autoantibodies (e.g anti-SLA)[22]. The
85 signature of these autoreactive CD4 T cells in the blood presented high similarity with the peripheral T
86 helper cells (T_{PH}) identified in the synovium of patients with rheumatoid arthritis and in other tissues
87 during autoimmunity[23–29]. However, it was still unknown whether the T_{PH} immune signature was a
88 common feature of other liver-self-antigen-specific CD4 T cells.

89 The similarity between circulating Sepsecs-specific CD4 T cells and T_{PH} in the tissue raised the question
90 whether circulating autoreactive CD4 T cells are directly linked to the reactivity in the tissue. Although
91 T_{PH} cells can also be found in smaller numbers in the blood, the site of their differentiation is
92 unknown[22,23,30]. In liver biopsies from AIH and PBC patients, Sepsecs- and PDCE2-reactive T cells are
93 detectable but poorly characterized; they produce TNF and/or INFγ[31–34]. Characterizing the immune
94 signature of T cells in tissues is a timely topic, but the dynamic link between tissues and circulation is

less well understood, particularly for CD4 T cells. Liver biopsies are small and rare, making it difficult to characterize liver-autoreactive CD4 T cells during AILD in the tissue. Thus, the capacity to detect in the blood autoreactive cells directly linked to tissue pathogenesis is an interesting perspective. Following an immune response or infection, peripheral CD4 and CD8 T cells can migrate into tissues to differentiate into tissue-resident memory (T_{RM}) cells that are characterized by clonal retention and segregation in the tissue[35,36]. Interestingly, T_{RM} CD4 T cells, T_{PH} cells and circulating Sepsecs-specific CD4 T cells express high levels of immune checkpoint molecules (PD-1, TIGIT and CTLA-4). This may suggest a tissue imprint of T_{PH} and Sepsecs-specific CD4 T cells found in the peripheral circulation due to chronic antigen stimulation in the tissue. We thus hypothesized that some circulating autoreactive CD4 T cell derive from an exacerbated clonal expansion in the tissue during active autoimmunity.

Here we used integrative single-cell immuno-transcriptomics to characterize three distinct liver-self-antigen-specific CD4 T cell reactivities and expanded intrahepatic CD4 T cell clonotypes in the blood of AILD patients. We revealed a shared signature and demonstrated that liver-autoreactive CD4 T cells can be detected in the peripheral bloodstream. In a mouse model designed to study the initiation of an immune response against an antigen expressed in the liver, we observed alterations of the transcriptomic profile of intrahepatic antigen-specific CD4 T cells after local antigen reactivity. The most relevant markers characterizing both intrahepatic and circulating liver-autoreactive CD4 T cells were the immune checkpoint molecules TIGIT, PD-1 and CTLA-4, which were involved in the control of local antigen-specific T cell reactivity. These results demonstrate how circulating liver-self-antigen-specific CD4 T cells are linked to tissue auto-reactivity and how the hepatic environment imprints their immune signature, with an important clinical perspective for monitoring and targeting liver auto-reactivity.

Results.

Self-antigen-specific CD4 T cell detection in AILD patients with auto-antibodies

We have previously shown that Sepsecs (SLA)-specific CD4 T cells are detectable in the blood of patients with autoimmune hepatitis (AIH) whose serum contains anti-SLA antibodies[22]. In the present study, we investigated whether we could extend those findings to autoreactive CD4 T cells specific for other antigens frequently targeted by autoantibodies in AILD. We studied the reactivity of CD4 T cells against Sepsecs, CYP2D6 and PDCE2 in AILD (AIH, PBC and overlap AIH/PBC) patients with or without anti-SLA (SLA^+) or anti-LKM1 ($LKM1^+$) or anti-M2 ($M2^+$) autoantibodies. As an experimental control, we also studied the reactivity of CD4 T cells against MP65 (Candida Albicans; C.ALB), MP1 (Influenza; H1N1) and SPIKE (SARS-CoV-2) in the AILD patients. As previously described[22], detection of antigen-specific CD4 T cells was achieved after four hours peptide stimulation *in vitro*. CD4 T cells that

specifically recognize antigen-derived peptides upregulate CD40 ligand (CD154) and can be detected by flow cytometry (Figure 1A and B). These reactive CD4 T cells were memory cells (CD45RA$^-$; mCD4 T cells) expressing high levels of PD-1 but not CXCR5 (Figure 1B and C). The frequency of Sepsecs-, CYP2D6- and PDCE2-specific PD-1$^+$ CXCR5$^-$ mCD4 T cells was significantly higher in patients with the presence of specific autoantibodies (Figure 1D). In comparison, the frequency of MP1 (H1N1)-, MP65 (C.ALB)- and SPIKE (SARS-CoV-2)-specific CD4 T cells was detectable in the blood of all patients (Figure 1E). Foreign antigen-specific CD4 T cells were also mCD4 T cells. MP1- and SPIKE-specific CD4 T cells expressed PD-1. Neither MP1-, MP65- or SPIKE-specific CD4 T cells expressed significant levels of CXCR5 (Figure 1E). In conclusion, during AILD, we observed an association between the specific autoimmune humoral response and the presence of circulating self-antigen specific CD4 T cells.

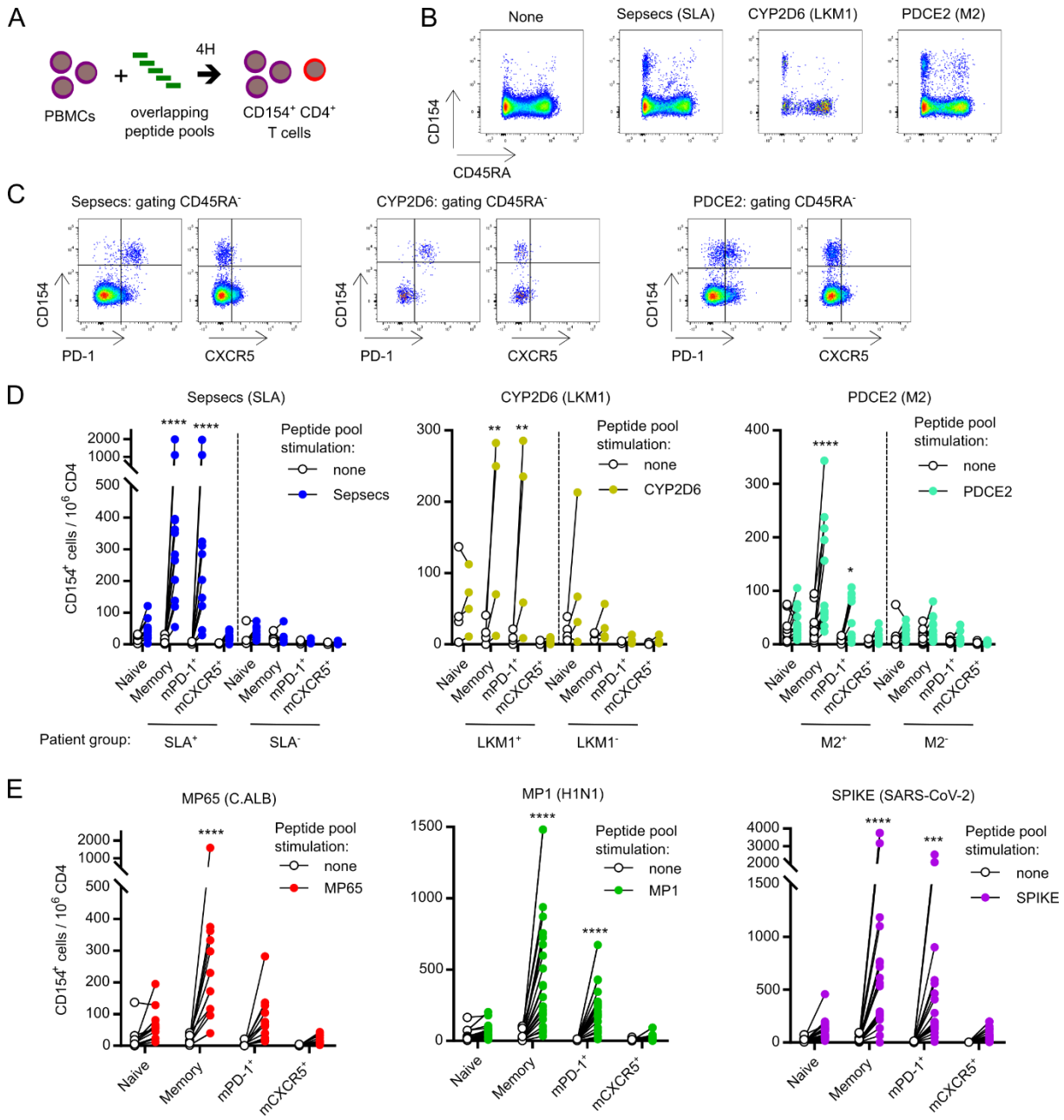

139 **Figure 1. Detection and immune-phenotyping of circulating liver-self-antigen-specific CD4 T cells.** (A) Schematic
140 representation of the detection of antigen-specific CD4 T cells based on the upregulation of CD40 ligand (CD154) after 4 hours
141 of *ex vivo* peptide stimulation. (B) Pseudocolor dot plot representation of CD45RA and CD154 expression at the surface of
142 CD4 T cells after stimulation with peptide pools from the indicated antigens. (C) Pseudocolor dot plot representation of PD-
143 1, CXCR5 and CD154 expression at the surface of CD45RA$^-$ mCD4 T cells after stimulation with peptide pools from the indicated
144 antigens. (D) Frequency of CD154$^+$ naïve, memory, memory PD-1$^+$ (mPD-1$^+$) and memory CXCR5$^+$ (mCXCR5$^+$) CD4 T cells per
145 million CD4 T cells after Sepsecs, CYP2D6 or PDCE2 peptides stimulation of PBMCs from 12 SLA$^+$ patients and 9 SLA$^-$ patients
146 (left); or 4 LKM1$^+$ patients and 4 LKM1$^-$ patients (central); or 14 M2$^+$ patients and 14 M2$^-$ patients (right). (E) Frequency of
147 CD154$^+$ naïve, memory, mPD-1$^+$ and mCXCR5$^+$ CD4 T cell per million CD4 T cells after MP65 (C.ALB), MP1 (H1N1) or SPIKE
148 (SARS-CoV-2) peptides stimulation of PBMCs from 13, 24 and 23 patients respectively. Sidak's multiple comparisons test was
149 used for D and E. *: $p<0.05$; **: $p<0.01$; ***: $p<0.001$; ****: $p<0.0001$.

150 ***Self-antigens-specific CD4 T cells have a unique transcriptomic immune signature during AILD***

151 We sorted self-antigen-specific and foreign antigen-specific mCD4 T cells by flow cytometry for single-
152 cell RNA-seq and TCR-seq analyses (Figure 2). An unsupervised clustering analysis led to the
153 identification of eight clusters (Figure 2A). The majority of transcriptional clusters corresponded to
154 distinct antigenic specificities rather than to distinct patients (Figure 2B and C). The only notable
155 exception was cluster 7, which corresponded to a PDCE2-specific CD4 T cell clonotype from one patient
156 (01-176) with a unique cytotoxic profile (Supplementary Figure 1).

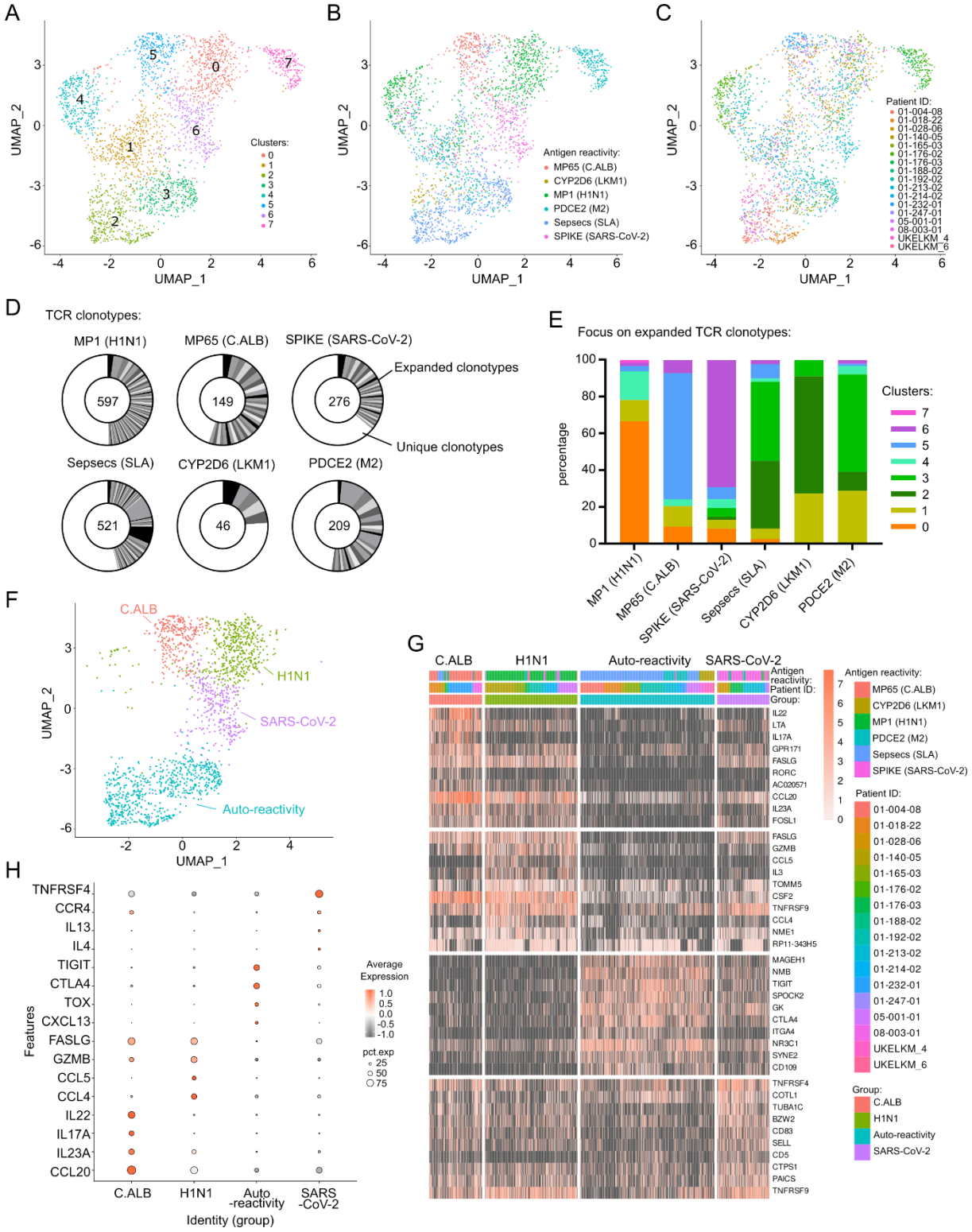

Figure 2. Single-cell RNA sequencing of liver-self-antigens specific CD4 T cells. A total of 2768 CD154⁺ mCD4 T cells (648 Sepsecs-, 113 CYP2D6-, 583 PDCE2-, 273 MP65-, 798 MP1- and 353 SPIKE-specific CD4 T cells) from 7 SLA⁺, 3 LKM1⁺ and 6 M2⁺ patients were analyzed for transcriptome and TCR sequences at the single cell level using FB5P-seq. (A) UMAP representation of antigen-specific memory CD4 T cell single-cell transcriptomes, colored by non-supervised Louvain cluster identity. (B) UMAP representation colored by antigen reactivity. (C) UMAP representation colored by patient ID. (D) TCRαβ clonal diversity of antigen-specific single T cells for each antigen- reactivity. Numbers indicate the number of single cells

analyzed with a TCRαβ sequence. Black and grey sectors indicate the proportion of TCRαβ clones (clonotype common to ≥ 2 cells) within single-cells analyzed; white sector: unique clonotypes. (E) Louvain cluster distribution of antigen-specific T cell clonotypes for each reactivity, as indicated. (F) UMAP representation of selected antigen reactivity cluster groups of memory CD4 T cells (C.ALB, H1N1, SARS-CoV-2 and auto-reactivity). (G) Single-cell gene expression heatmap for top 10 marker genes of cells from each antigen reactivity group defined in (F). (H) Dot plot representation of four selected marker genes of clusters C.ALB, H1N1, SARS-CoV-2 and auto-reactivity.

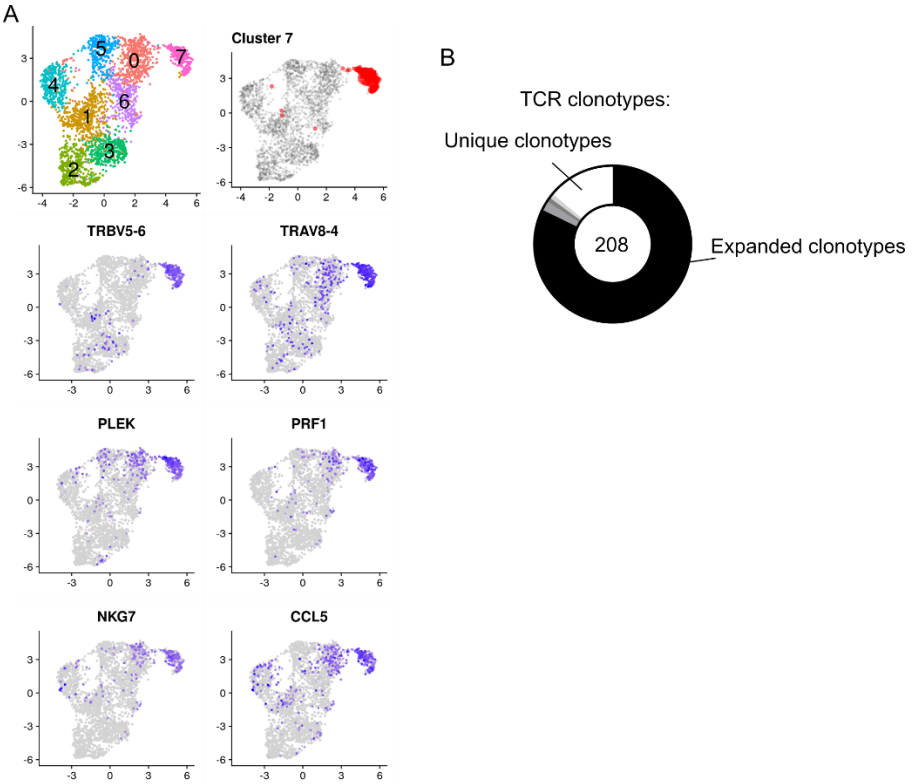

Supplementary figure 1: Characterization of the cluster 7 of PDCE2-specific CD4 T cells. (A) UMAP representation of selected gene markers. (B) TCRαβ clonal diversity of antigen-specific single T cells for cluster 7 cells. Numbers indicate the number of single cells analyzed with a TCRαβ sequence. Black and grey sectors indicate the proportion of TCRαβ clones (clonotype common to ≥ 2 cells) within single-cells analyzed; white sector: unique clonotypes.

As the memory response against an antigen is generally associated with clonal expansion, we analyzed the diversity and proportion of TCR clonotypes for each antigen reactivity (Figure 2D). Clonal expansion was observed for every antigenic reactivity, whether associated with self- or foreign-reactivity. Analysis of these expanded clones for cluster affiliation demonstrated that transcriptional clusters were linked to antigenic reactivity (Figure 2E). Interestingly, all three liver auto-reactivities were grouped in the same clusters. Sepsecs-, CYP2D6- and PDCE2-specific CD4 T cells were in the clusters 2 and 3. MP1-specific CD4 T cells were in the cluster 0; MP65-specific CD4 T cells were in the cluster 5; and SPIKE-specific CD4 T cells were in the cluster 6. Two clusters (4 and 1) were not linked to antigenic reactivity. We annotated four antigen-reactivity groups based on unsupervised transcriptional clustering: the H1N1 cluster (ex-cluster 0); the C.ALB cluster, (ex-cluster 5); the SARS-CoV-2 cluster (ex-cluster 6); and

185 the auto-reactivity cluster (ex-clusters 2 and 3) (Figure 2F and G). The gene signature of autoantigen-
186 reactive cells was linked to the regulation of T cell activation and immune exhaustion (*CTLA-4, TIGIT,*
187 *BATF, IL21, CD74, PRDM1, TOX*). This gene signature, together with the *CXCL13* gene, was also linked
188 to the B-helper autoreactive signature of T_{PH} described in other autoimmune disorders (Figure 2H). In
189 comparison, the H1N1 gene signature was associated with a classical antiviral response and T cell
190 chemotaxis (*GZMB*, *CCL4, CCL5 and FASLG*). The Candida Albicans gene signature was associated with
191 a type 17 helper response (*CCL20, IL22, IL17A, IL23A*). SARS-CoV-2 gene signature was associated with
192 a type 2 helper response and B cell activation (*TNFRSF4, CCR4, IL4 and IL13*). We had the opportunity
193 to longitudinally analyze the TCR clonotypes of Sepsecs-specific and MP65-specific CD4 T cells of
194 patients (n=3 and 1, respectively) over 3 years (2018 to 2021). Although variable numbers of novel
195 clones were detected in patients' blood over time, some conserved Sepsecs-specific CD4 T clonotypes
196 were detected over the 3-year period (Supplementary Figure 2), suggesting chronically active clonal
197 expansion of autoreactive CD4 T cells despite their immuno-exhausted molecular profile. Altogether,
198 these data demonstrate that distinct liver-self-antigen-specific CD4 T cells had a common specific B-
199 helper autoreactive signature, with high-level expression of checkpoint inhibitors (immuno-exhausted
200 transcriptional profile).

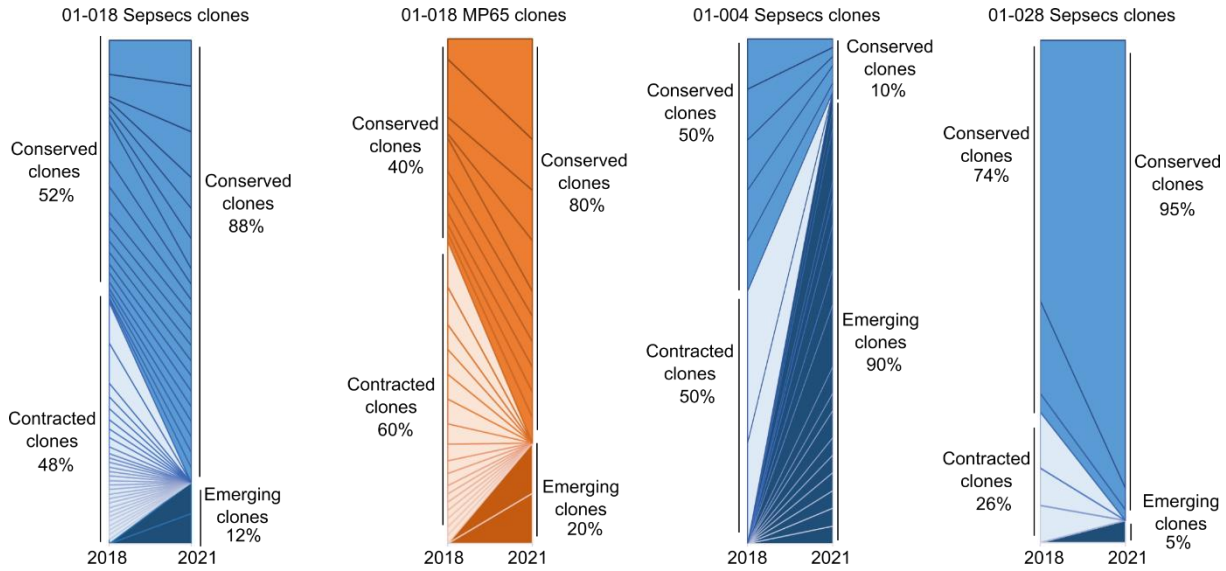

201

202 **Supplementary figure 2: Longitudinal analysis of Sepsecs-specific clonotypes.** Representation of the proportion of Sepsecs-
203 and MP65-clonotypes between 2018 and 2021 in the blood of three patients.

204 ***Clonal overlap between circulating autoreactive and intra-hepatic CD4 T cells in AILD***

205 We then attempted to answer the following question: how related to liver infiltrating CD4 T cells are
206 circulating autoreactive CD4 T cells in AILD? We hypothesized that circulating autoreactive CD4 T cells
207 might represent clonal relatives of liver CD4 T cells and that their specific molecular profile was induced
208 during chronic antigen reactivity in the tissue. For one SLA^+ patient analyzed by peptide restimulation

209 and single-cell sequencing (Figure 2, patient 01-192), we also had access to a frozen liver biopsy, from
210 which we derived bulk TCR-beta-seq data (Supplementary Figure 3A). Six out of sixty (10%) Sepsecs-
211 specific circulating CD4 TCR clonotypes were also detected in the liver, compared to only one out of
212 forty-six (2.2%) MP1-specific TCR clonotypes (H1N1). Bulk TCR-beta sequence counts corresponding to
213 Sepsecs-specific clonotypes suggested few clonal expansions dominating the Sepsec-specific response
214 also in the liver (Supplementary Figure 3C). Thus, for this patient, circulating self-antigen-specific CD4
215 T cells reflected clonally expanding autoantigen-specific T cells within the liver.

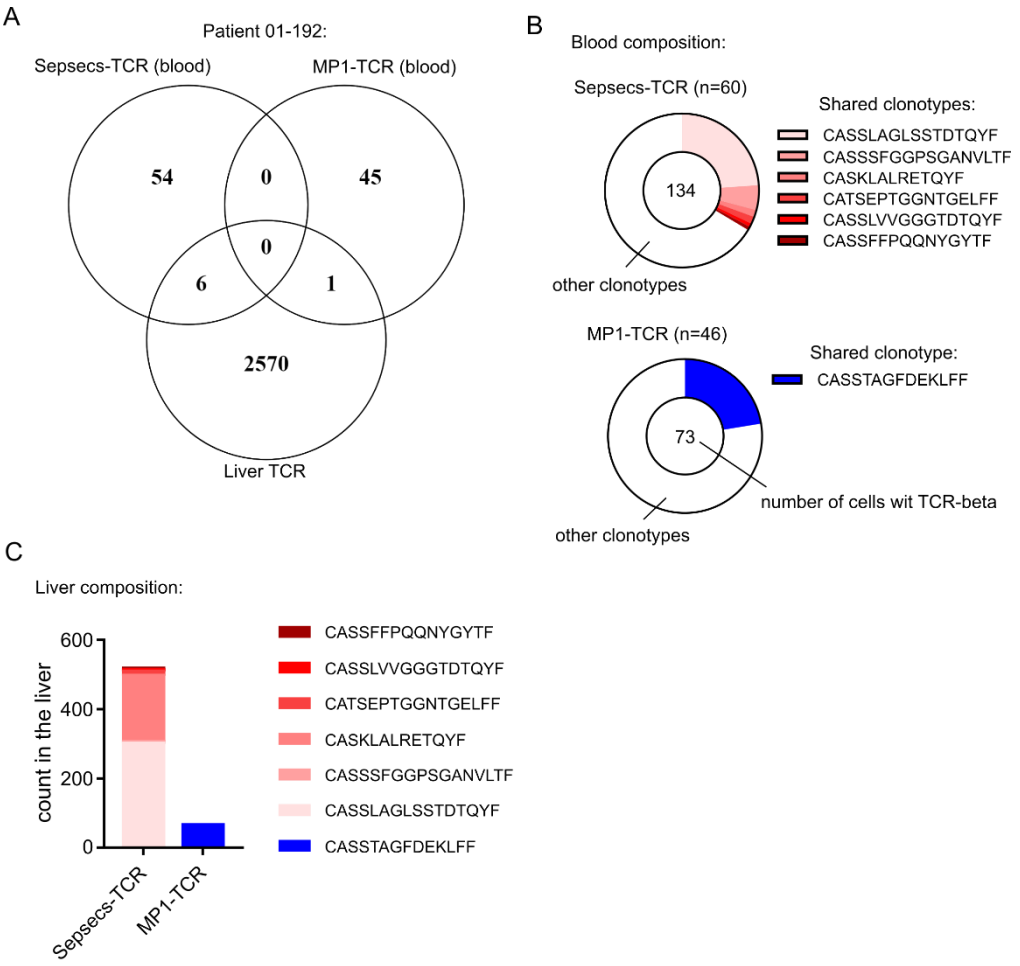

216

217 **Supplementary figure 3: Sepsecs-clonotypes are enriched in the liver of an SLA⁺ patient.** (A) Shared TCR between Sepsecs-
218 specific CD4 T cells, MP1-specific CD4 T cells and the liver biopsy. (B) Proportion of shared TCR with the liver (colored sectors)
219 within TCRαβ clonal diversity of Sepsecs- or MP1-specific CD4 T cells. (C) Liver frequency (count) of shared-TCRβ sequences.

220 For most AILD patients, no self-antigen reactive TCR were known. Therefore, to continue exploring the
221 relationship between circulating and liver CD4 T cells, we took advantage of our initial observation that
222 in AILD, most circulating self-antigen-specific CD4 T cells have a PD-1^{+} CXCR5^{-} CD45RA^{-} memory
223 phenotype[22] (Figure 1). We had access to paired blood-liver samples from 4 AILD patients; for each,
224 we extracted genomic DNA and performed bulk TCR-beta-seq from blood PD-1^{+} CXCR5^{-} mCD4 T cells,
225 blood PD-1^{-} mCD4 T cells, and whole liver biopsy (Supplementary Figure 4A). First, we observed that

226 the 100 most abundant TCR-beta sequences in the liver account for more than 50% of intrahepatic
227 TCRs, suggesting strong local clonal expansion (Supplementary Figure 4B). We also observed that the
228 PD-1^{+} CXCR5^{-} mCD4 T cell population shared more TCR-beta sequences with the liver than PD-1^{-} mCD4
229 T cells (Supplementary Figure 4C). Interestingly, the proportion of cells with the top 100 liver TCR-beta
230 sequences was high in the PD-1^{+} CXCR5^{-} mCD4 T cell population, than in the PD-1^{-} mCD4 T cells
231 (supplementary Figure 4D). This data demonstrated the circulating PD-1^{+} CXCR5^{-} mCD4 T cell
232 population contain dominant intrahepatic CD4 T cell clonotypes.

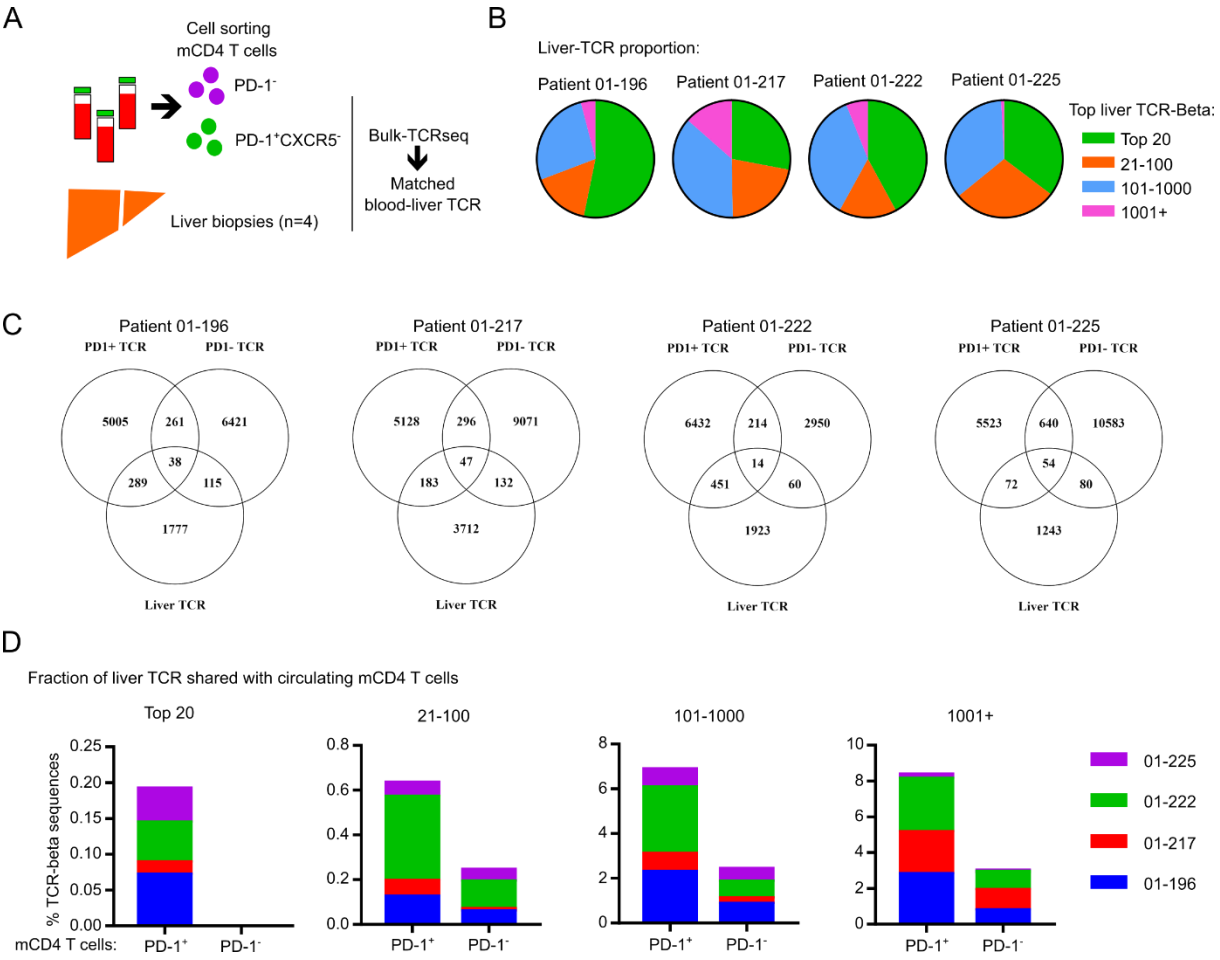

233

234 **Supplementary figure 4: Shared TCRβ sequences between Blood PD-1^{+} or PD-1^{-} CD4 T cells and the liver biopsies from four**
235 **distinct patients**. (A) Experimental design for bulk TCRβ sequencing. (B) Pie chart showing the proportion of the TCRβ
236 repertoire occupied by the top 20, 100, 1000 or 1001+ clones. (C) Shared TCRβ sequences between Blood PD-1^{+} or PD-1^{-}
237 mCD4 T cells and the liver biopsies from the four distinct patients. (D) Analysis of the percentage of TCRβ clonotypes shared
238 between the top 20, 100, 1000 or 1001+ liver clones and the circulating PD-1^{+} CXCR5^{-} (PD-1^{+}) or PD-1^{-} mCD4 T cells (PD-1^{-})
239 from four distinct AILD patients.

240 Based on this, we performed droplet-based single-cell RNA-seq combined with TCR sequencing of
241 blood PD-1^{+} CXCR5^{-} mCD4 T cells from the four patients to characterize the transcriptional profile of
242 cells with TCR clonotypes detected in the matched liver biopsies (Figure 3A). First, cluster analysis of
243 PD-1^{+} CXCR5^{-} mCD4 T cells revealed the heterogeneity of these cells (Figure 3B). The main subsets

244 identified by unsupervised azimuth annotation and marker gene analysis were: *GZMK*$^{+}$ effector CD4 T
245 cells (T_{EM} GZMK^{+}, cluster 1); *HLA-DR*$^{+}$ recently activated central memory CD4 T cell (T_{CM} HLA-DR^{+}, cluster
246 2), *NKG7*$^{+}$ effector CD4 T cell (T_{EM} NKG7^{+}, clusters 3); cytotoxic (*GZMB*$^{+}$*GNLY*$^{+}$) CD4 T cells (CTL, clusters
247 5) and *FOXP3*$^{+}$ (regulatory) CD4 T cell (T_{REG}, cluster 6) (Figure 3B and C, and supplementary Figure 5 and
248 6). Clusters 4, 7 and 8 were likely subsets of T_{CM} but were difficult to further annotate based on marker
249 genes.

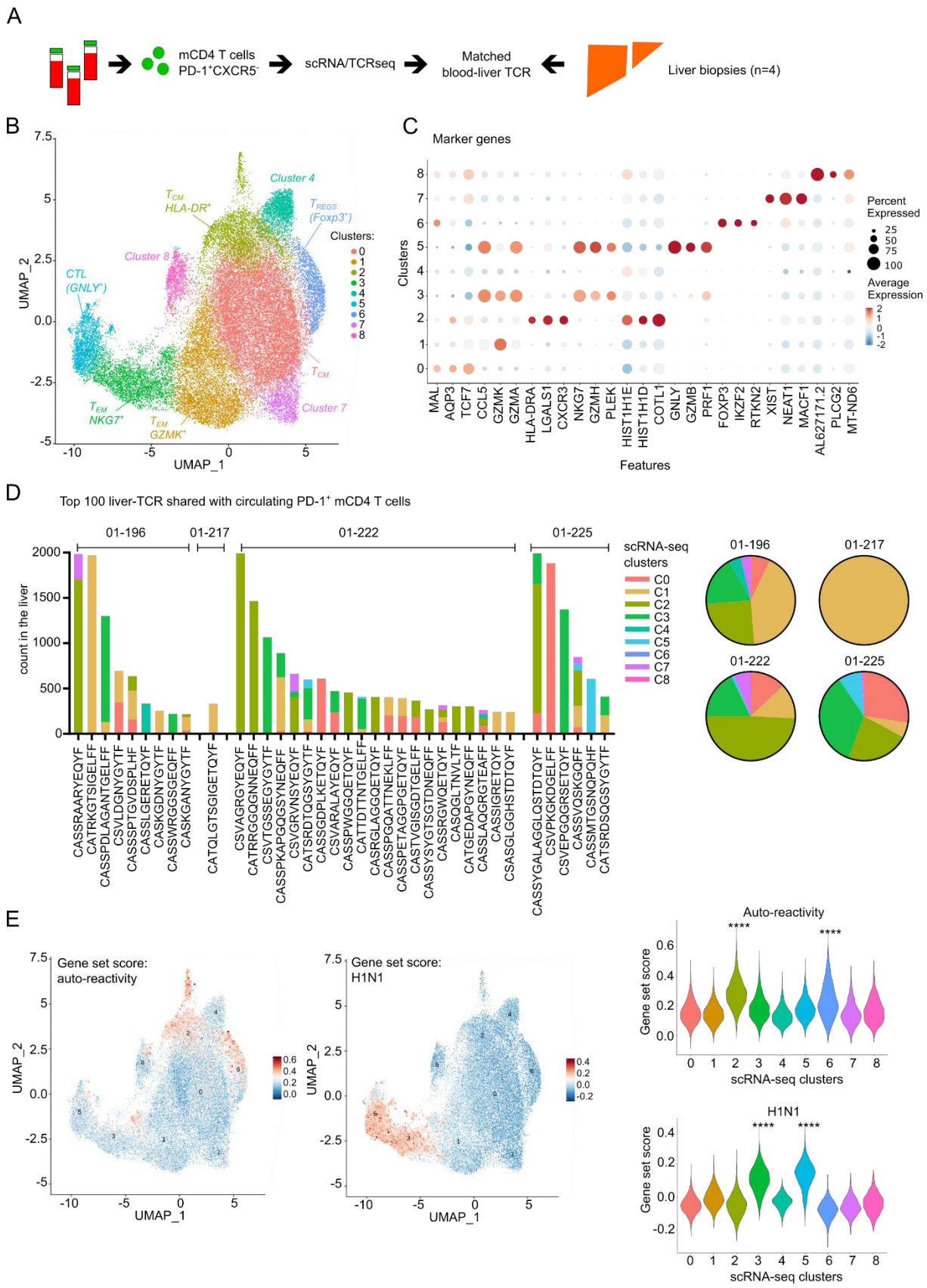

Figure 3. Tracking TCR clonotypes between liver biopsies and circulating CD4 T cell subsets. (A) Experimental design for scRNA-seq and TCR-seq of memory PD-1^{+} CXCR5^{-} CD4 T cells from four distinct AILD patients. (B) UMAP representation of circulating memory PD-1^{+} CXCR5^{-} CD4 T cell transcriptomes, colored by non-supervised Louvain clustering. (C) Dot plot

representation of top 3 marker genes of each clusters in (B). (D) Frequency representation ('counts') of each top 100 largest liver TCRβ sequences found in circulating PD-1$^+$ mCD4 T cells. For each TCRβ sequences the cluster affiliation is indicated based on scRNA-seq and TCR-seq of memory PD-1$^+$ CXCR5$^-$ CD4 T cells. Pie chart represent the global cluster affiliation of the top 100 largest liver TCRβ sequences found in circulating PD-1$^+$ mCD4 T cells per patient. (E) Left: UMAP representation of circulating memory PD-1$^+$ CXCR5$^-$ CD4 T cell transcriptomes colored by gene set score for the indicated antigen-reactivity module. Right: violin plots of gene set score distribution of cells from different Louvain clusters, as indicated. Pairwise comparison with Benjamini-Hochberg corrected Wilcoxon test. ****: $p<0.0001$.

In this data set, we tracked the top 100 liver TCR-Beta sequences (Figure 3D). For each of these liver TCR-beta clones, we assigned a cluster identification based on single-cell transcriptomic data from PD-1$^+$ CXCR5$^-$ mCD4 T cells (Figure 3D). The analysis revealed top expanded intrahepatic clones found in the blood were mainly distributed between cluster 1 (T_{EM} GZMK$^+$), cluster 2 (T_{CM} HLA-DR$^+$) and cluster 3 (T_{EM} NKG7$^+$). We computed gene set scores based on our analyses of peptide-stimulated T cells (Figure 2), with the expression of the top 50 genes (avg_log2FC) from auto-reactivity or H1N1 reactivity, respectively. These scores were then quantified in the droplet-based scRNA-seq dataset of non-stimulated PD-1$^+$ CXCR5$^-$ mCD4 T cells (Figure 3E). Cells in cluster 2 (T_{CM} HLA-DR$^+$) had the highest score for the auto-reactivity module, while cells in clusters 3 and 5 had the highest score for the H1N1 module. These data suggest that cells in cluster 2, PD-1$^+$ CXCR5$^-$ HLA-DR$^+$ T_{CM}, were the main circulating CD4 T cell clonal counterpart of liver-autoreactive CD4 T cells. Interestingly, this cluster 2 also contained proliferative CD4 T cells, reinforcing the idea of local clonal expansion (Supplementary Figure 6).

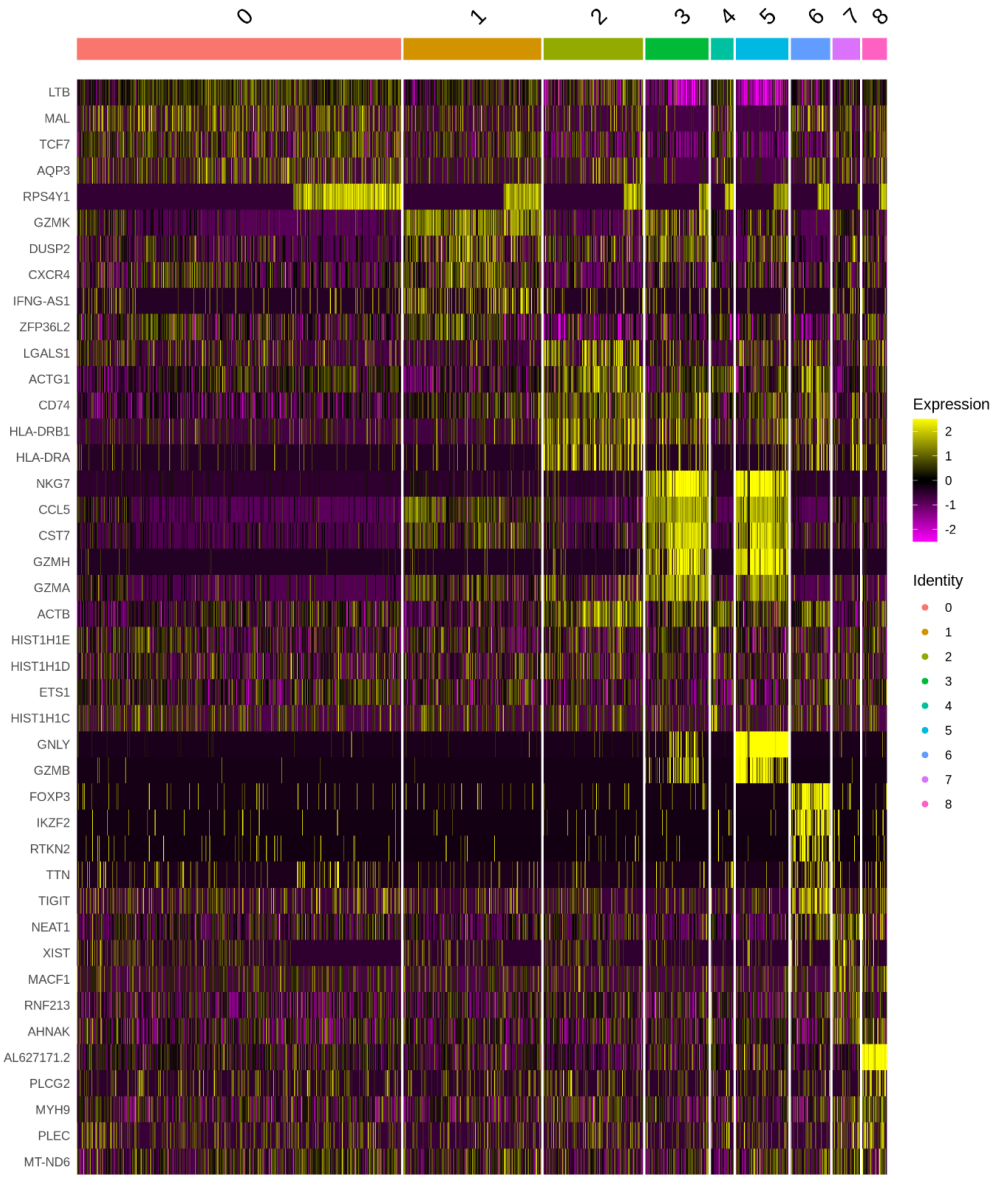

Supplementary figure 5: Single cell gene expression heatmap for top 5 marker genes of PD-1^{+} CXCR5^{-} memory CD4 T cells.

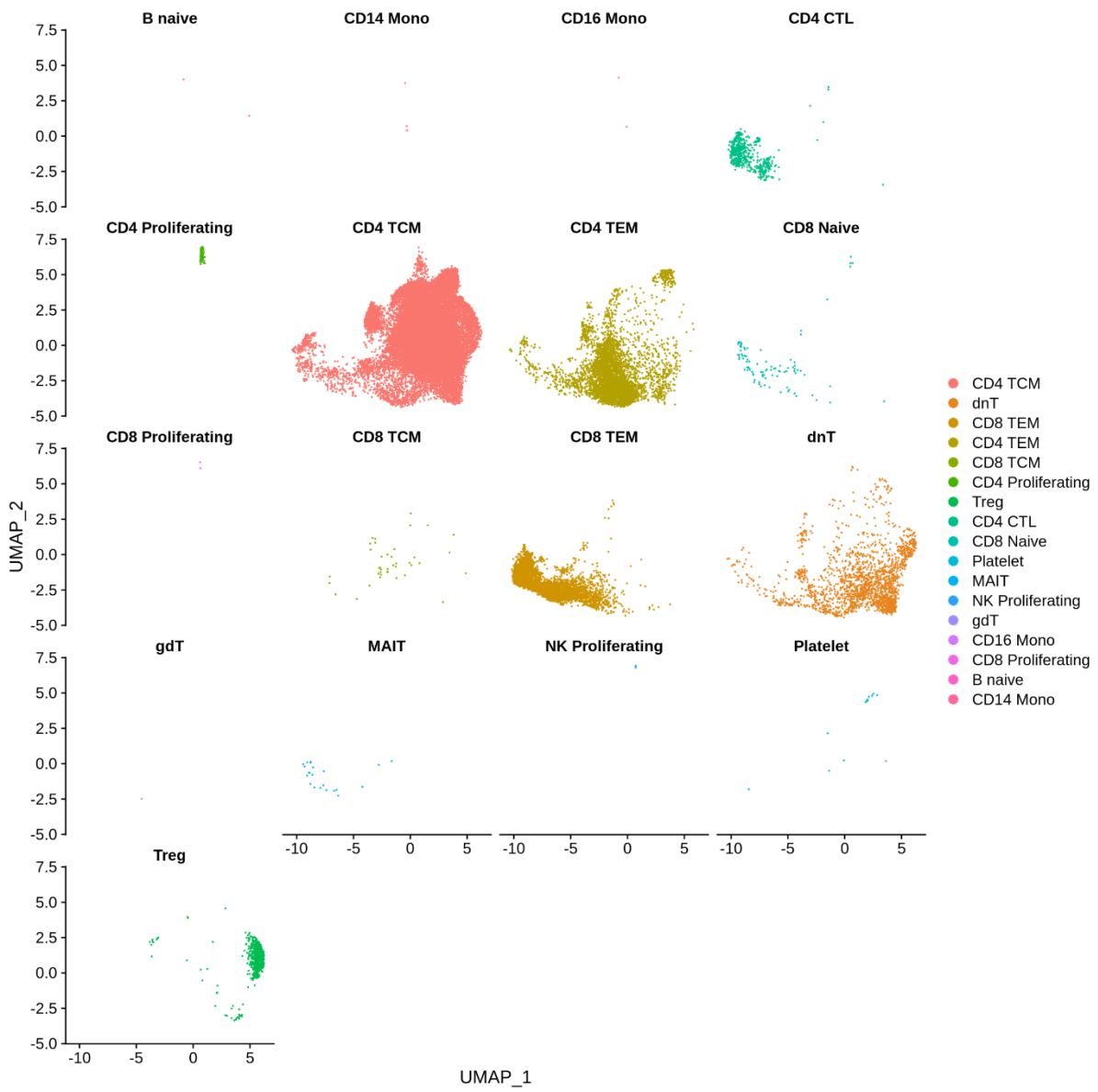

Supplementary figure 6: Unsupervised azimuth annotation of scRNA-seq data from PD-1⁺ CXCR5⁻ memory CD4 T cell subsets.

We further sought to relate the transcriptional signatures of peptide-stimulated and untouched circulating autoreactive mCD4 T cells (Figure 2 and 3). Based on previously published results[22], we synthesized HLA-DRB1 03:01 biotinylated monomers loaded with the $Sepsecs_{187\text{-}197}$ epitope peptide, assembled fluorescent-labeled pMHCII tetramers, and monitored Sepsecs-specific CD4 T cells in the blood of six SLA^{+} $HLA\text{-}DR3^{+}$ patients (Figure 4A). Peptide-MHCII tetramer positive (TTpos) CD4 T cells were detectable and displayed a $PD\text{-}1^{+}$ memory phenotype (Figure 4B). We performed plate-based single-cell transcriptomic analyses of pMHCII TTpos Sepsecs-specific CD4 T cells. We compared pMHCII TTpos and TTneg CD4 T cells for their expression of gene modules associated with antigen reactivities defined in Figure 2 (Figure 4C) and in the $PD\text{-}1^{+}$ $CXCR5^{-}$ mCD4 T cell subsets identified in Figure 3 (Figure

288 4D). As expected, pMHCII TTpos CD4 T cells expressed significantly higher levels of gene modules
289 associated to self-antigen specific CD4 T cells (Figure 4C) and cluster 2 T_{CM} HLA-DR$^+$ CD4$^+$ cells (Figure
290 4D).

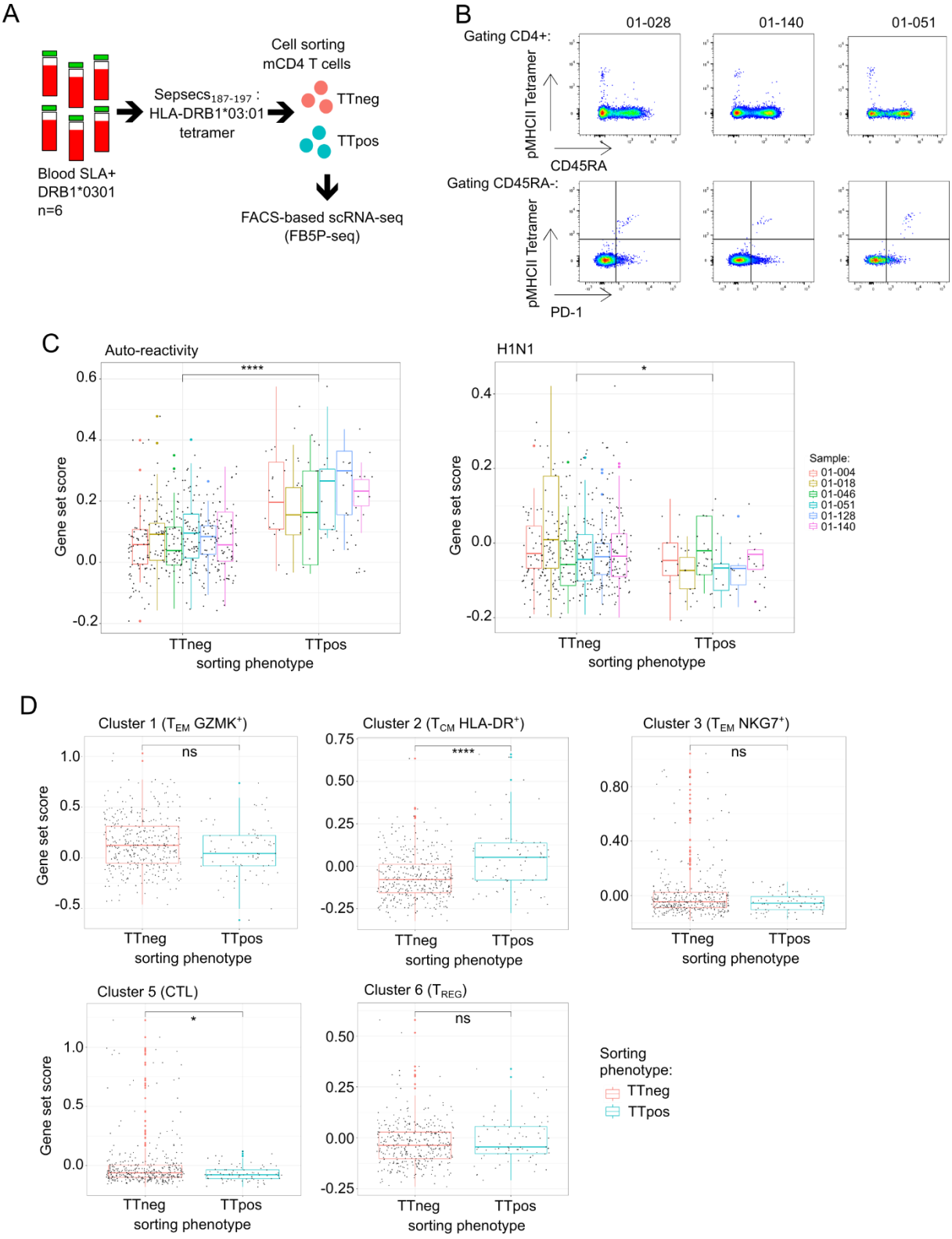

291

292 **Figure 4. Single cell transcriptomic analysis of unstimulated Sepsecs-specific CD4 T cells.** (A) Experimental design for scRNA-
293 seq data analysis of Sepsecs/SLA$_{185-197}$ HLA-DRB1*0301 pMHCII tetramer positive cells. (B) Pseudocolor dot plot

294 representation of pMHCII tetramer staining in three of six patients. Top: surface expression of CD45RA and pMHCII tetramer
295 in $CD4^+$ T cells. Bottom: surface expression of PD-1 and pMHCII tetramer in $CD4^+$ $CD45RA^-$ T cells. (C) Box plots of gene set
296 score distribution of pMHCII tetramer negative (TTneg) or positive (TTpos) cells for antigen reactivity modules as indicated.
297 (D) Box plots of gene set score distribution of pMHCII tetramer negative (TTneg) or positive (TTpos) cells for top marker genes
298 of circulating memory PD-1^+ $CXCR5^-$ CD4 T cell clusters defined in Figure 3E. Unpaired Mann-Whitney test was used: *: $p<0.05$;
299 ****: $p<0.0001$.

300 Altogether, our integrative analyses of circulating self-antigen-specific and dominant intrahepatic CD4
301 T cell clones in AILD patients converge to establish that some autoreactive CD4 T cell clones can be
302 found both in the liver and in the blood, where they are defined as PD-1^+ $CXCR5^-$ HLA-DR^+ mCD4 T cells,
303 with a specific B-helper and immuno-exhausted transcriptional profile.

304 ***High-dimensional phenotyping of circulating liver-autoreactive CD4 T cells***

305 We then examined the precise phenotype of these circulating liver-autoreactive CD4 T cells by spectral
306 flow cytometry using PBMCs from patients affected by different liver diseases: five control non-
307 autoimmune patients with non-alcoholic steatohepatitis (NASH), fourteen AIH patients with an active
308 disease, and thirteen AIH patients in remission under treatment (Supplementary Table 2). We focused
309 on the mCD4 T cell population and performed clustering analysis (Figure 5A-D). The comparison
310 revealed the significant increase of three cell clusters in patients with active AIH in comparison to NASH
311 patients (C6, C12 and C15, Figure 5B). The C6 and C15 clusters were T_{CM} $CD27^+$ $TIGIT^+$ PD-1^+ $CXCR5^-$
312 $CD49d^+$ $CD25^-$ $CD127^-$ $ICOS^+$ CD4 cells and expressed CD38, a marker we have already observed
313 upregulated by CD4 T cells during active AIH[22] (Figure 5C and D, Supplementary Figure 7).The C15
314 cluster was characterized by high HLA-DR expression and may represent the liver-autoreactive CD4 T
315 cells identified previously (Figure 3). This cluster (C15) was high in the blood of active AIH patients
316 compared to AIH patients in remission under treatment (Supplementary Figure 7). The C12 cluster was
317 characterized by CD57 expression but its frequency was very low. We performed a supervised analysis
318 of the HLA-DR^+ subset and confirmed that it was significantly more frequent during the active phase
319 (AIHa) than in patients with NASH or in remission (AIHr) (Supplementary Figure 8). In parallel, in four
320 active AIH patients, we performed the intracellular analysis of the PD-1^+ $TIGIT^+$ $CXCR5^-$ CD4 subset with
321 a new panel of antibodies. We confirmed its heterogeneity; this subset consisted of classical T_{REG}
322 ($FOXP3^+$ $CD127^-$ $EOMES^-$), cytotoxic cells ($GZMB^+$ HLA-DR^- $EOMES^+$ $GZMA^+$) and HLA-DR^+ $FOXP3^-$ $EOMES^-$
323 cells (Supplementary Figure 9). This was in agreement with the transcriptomic data (Figure 3) to
324 demonstrate that the liver-autoreactive CD4 T cell cluster (HLA-DR^+ PD-1^+) was different from the T_{REG}
325 and cytotoxic (CTL) PD-1^+ CD4 T cell clusters. Thus, after exclusion of T_{REGs} (using CD127 and CD25 or
326 FOXP3 expression), HLA-DR expression emerged as the most relevant marker for delineating liver-
327 autoreactive CD4 T cells among PD-1^+ $TIGIT^+$ CD4 T cells.

328

Group	Active AIH (AIHa)	Remission AIH (AIHr)	NASH
	n=14	n=13	n=5
Age (year)	50,3 [39,7-61]	52,5 [39,1-65,8]	59,2 [33,3-85,1]
Female, n (%)	9 (64%)	9 (69%)	3 (60%)
IgG (g/L)	19,5 [15,2-23,8]	11,4 [9,9-12,9]	11,9 [6,8-17,1]
AST (IU/L)	307 [121,7-492,1]	22,6 [17,4-27,9]	45,9 [23,4-68,4]
ALT (IU/L)	505 [185,6-824,7]	20,8 [14,4-27,1]	73,5 [6,2-140,9]
Immunosuppressive agents n (%)			
No, n (%)	9 (64%)	0	5 (100%)
Naïve	9	0	NA
Yes, n (%)	5 (36%)	13 (100%)	0
Azathioprin	4	11	NA
MMF	1	1	NA
Steroids only	0	1	NA
Steroids associated to other therapy	2	3	NA

329 *AIH: Autoimmune Hepatitis, NASH: Non Alcoholic Steatohepatitis, AST: Aspartate Aminotransferase, ALT: Alanine*
330 *Aminotransferase, NA: non-applicable*

331 **Supplementary Table 2**. Clinical and biological characteristics of patients with AIH and NASH expressed as mean [95%
332 confidence interval].

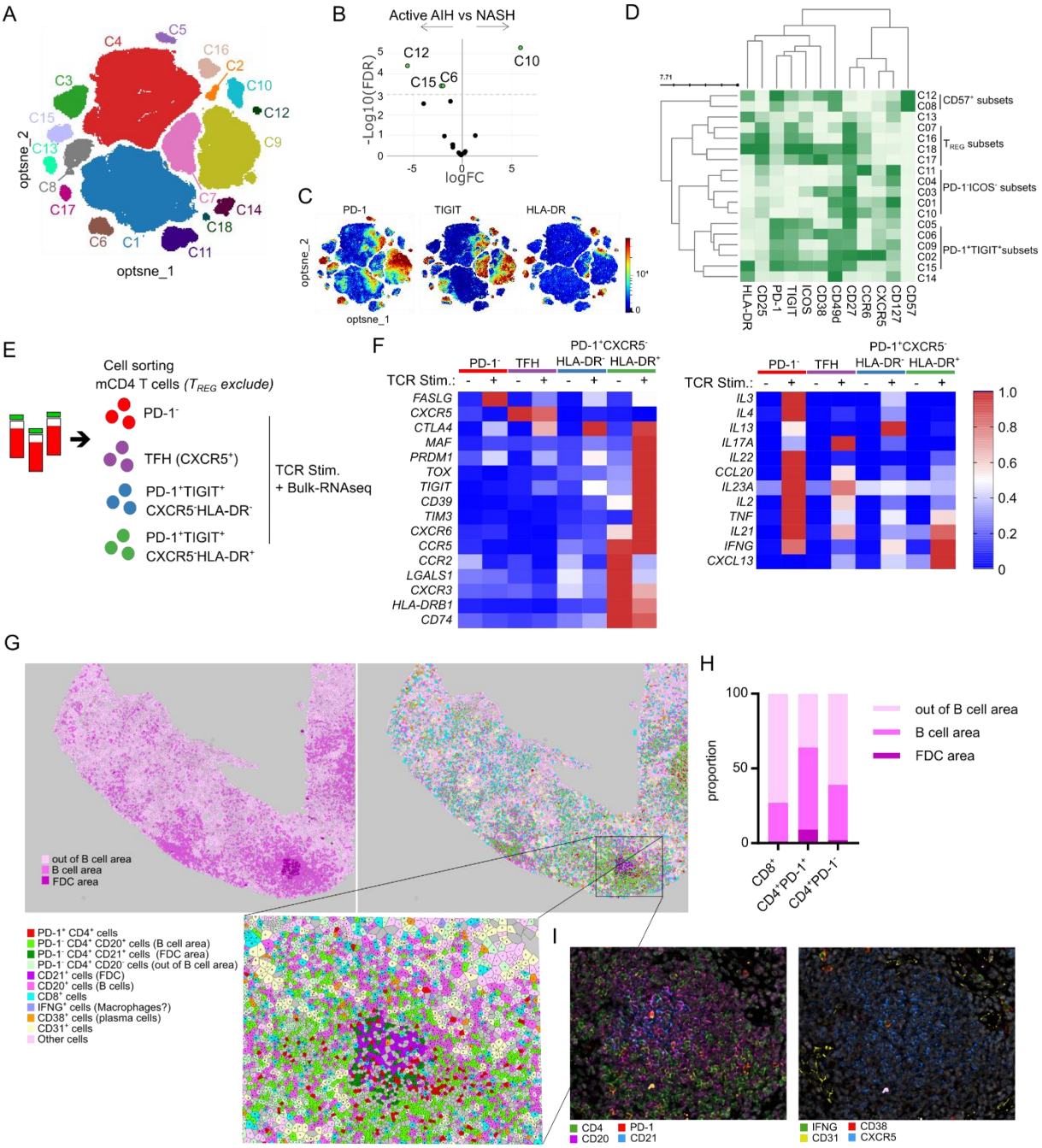

Figure 5: Characterization of circulating PD-1⁺ TGIT⁺ HLA-DR⁺ non-T_{REG} CD4 T cells as liver-autoreactive CD4 T cells. (A) opt-SNE representation of blood memory CD4 T cell subsets, colored by non-supervised FlowSOM clustering, from 5 control non-autoimmune patients with non-alcoholic steatohepatitis (NASH), 14 AIH patients with an active disease (Active AIH), and 13 AIH patients in remission under treatment. (B) Differential cluster abundance between active AIH and NASH patients. (C) PD-1, TIGIT and HLA-DR expression. (D) Surface marker heatmap of the clusters identified in (A). (E) Experimental design for bulk-RNA-seq after cell sorting and 24h *in vitro* TCR stimulation. (F) Selected genes heatmap of indicated CD4 T cell subsets after or not TCR stimulation from five distinct patients (mean representation). (G) Voronoi representation of cellular subsets in an AIH liver biopsy after cell segmentation. FDC area is defined by expression of CD21; B cell area is defined by CD20 expression; and out of B cell area is defined by the absence of CD20 expression. The lower panel shows a zoom on the selection indicated in the upper panel. (H) Representation of the repartition of CD8⁺, CD4⁺ PD-1⁺ and CD4⁺ PD-1⁻ cells in FDC, B cell and out of B cell area defined in (G). (I) CD4, CD20, PD-1, CD21, IFNγ, CD38, CD31 and CXCR5 marker staining within segmentation.

345 To get an insight into the functionality of these rare cells, we used this strategy of T_{REG} exclusion to sort
346 HLA-DR$^+$ PD-1$^+$ TIGIT$^+$ CXCR5$^-$ mCD4 T cells and to perform their TCR stimulation *in vitro* for bulk-RNA
347 sequencing (Figure 5E and F). Like autoreactive CD4 T cells after peptide stimulation, HLA-DR$^+$ PD-1$^+$
348 TIGIT$^+$ CXCR5$^-$ mCD4 T cells significantly upregulated *CXCL13*, *IL21*, *CTLA-4*, *PRDM1*, *TIGIT*, *MAF* and
349 *TOX,* upon TCR stimulation. These cells also expressed *LGALS1*, *CXCR3, HLA-DR and CD74* like CD4 T_{CM}
350 HLA-DR$^+$ cells*;* these genes were downregulated by TCR stimulation. They expressed genes associated
351 to the T_{PH} and T_{RM} CD4 cell signature like *ENTPD1, TIM3, CXCR6, CCR5* and *CCR2* that linked them to
352 the tissue immune response. They could also express *TNF* and *INFG*, but not *IL2*, after TCR stimulation.
353 This subset presented high proximity with autoreactive CD4 T cells and circulating dominant
354 intrahepatic clonotype, thus, we can conclude that HLA-DR$^+$ PD-1$^+$ TIGIT$^+$ CXCR5$^-$ CD4 T cells contained
355 the liver-autoreactive CD4 T cells.

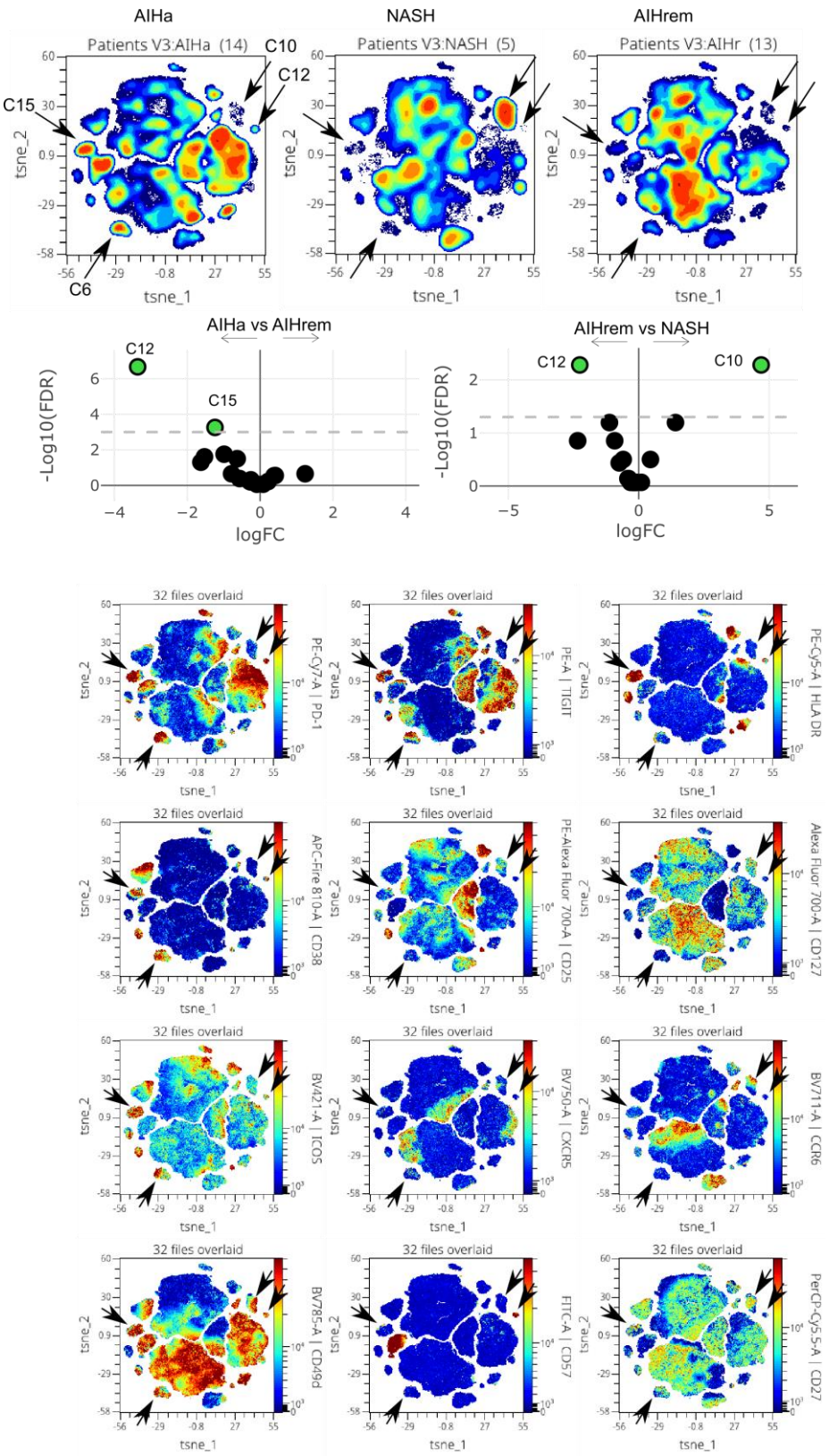

Supplementary figure 7: Detailed unsupervised flow cytometry analysis of active AIH (AIHa), NASH and AIH in remission (AIHrem) patients and expression of indicated markers on the opt-SNE representation of blood memory CD4 T cell subsets.

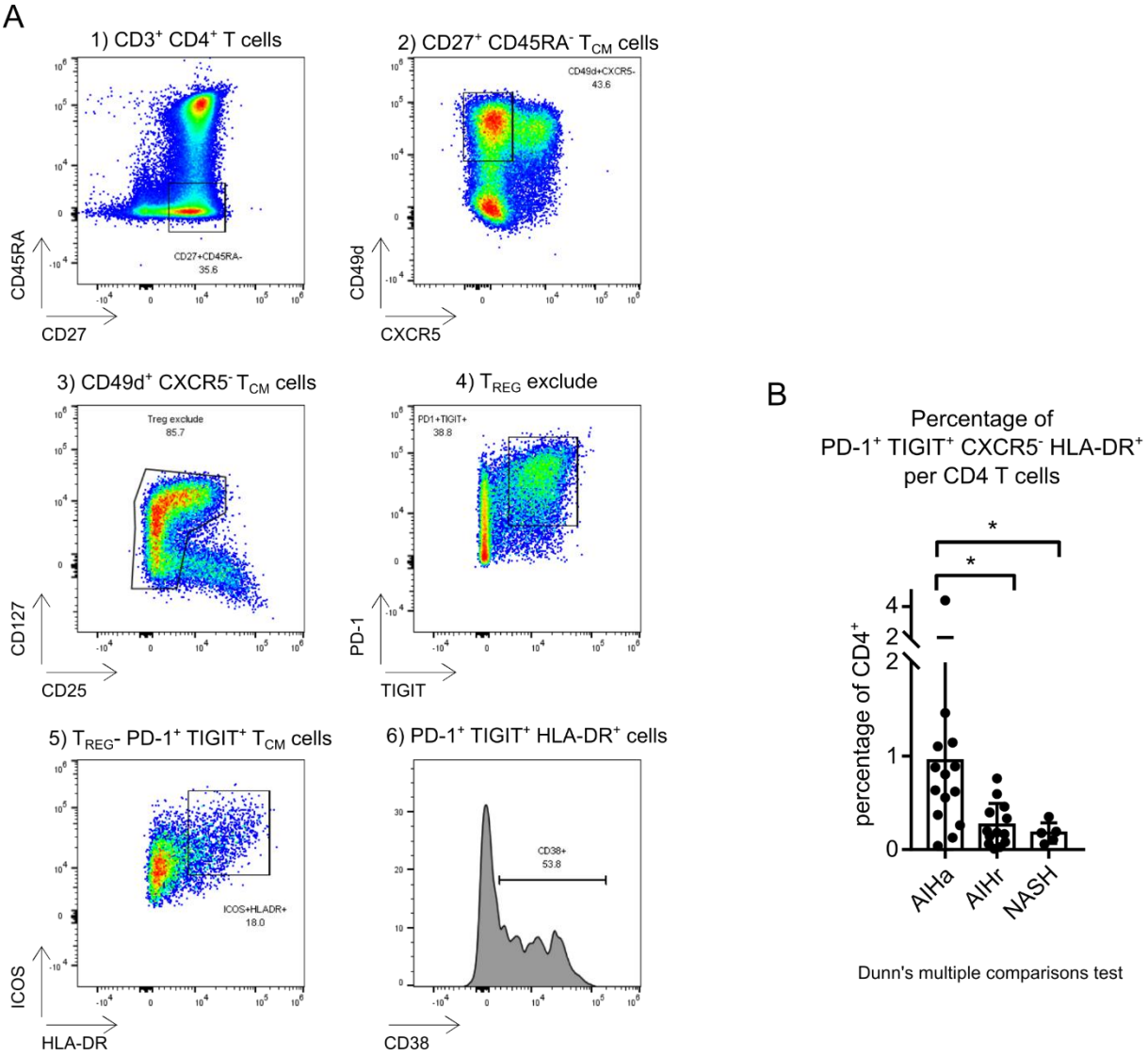

Supplementary figure 8: Supervised identification of the cluster 08 (PD-1⁺ CXCR5⁻ TIGIT⁺ HLA-DR⁺). (A) dot plot representation of the gating strategy. (B) Frequency of PD-1⁺ CXCR5⁻ TIGIT⁺ HLA-DR⁺ CD4 T cells per total CD4⁺ T cells in the blood of 5 NASH, 14 active AIH (AIHa), and 13 AIH patients in remission (AIHr) under treatment (<2 years, n=4; >2years, n=12).

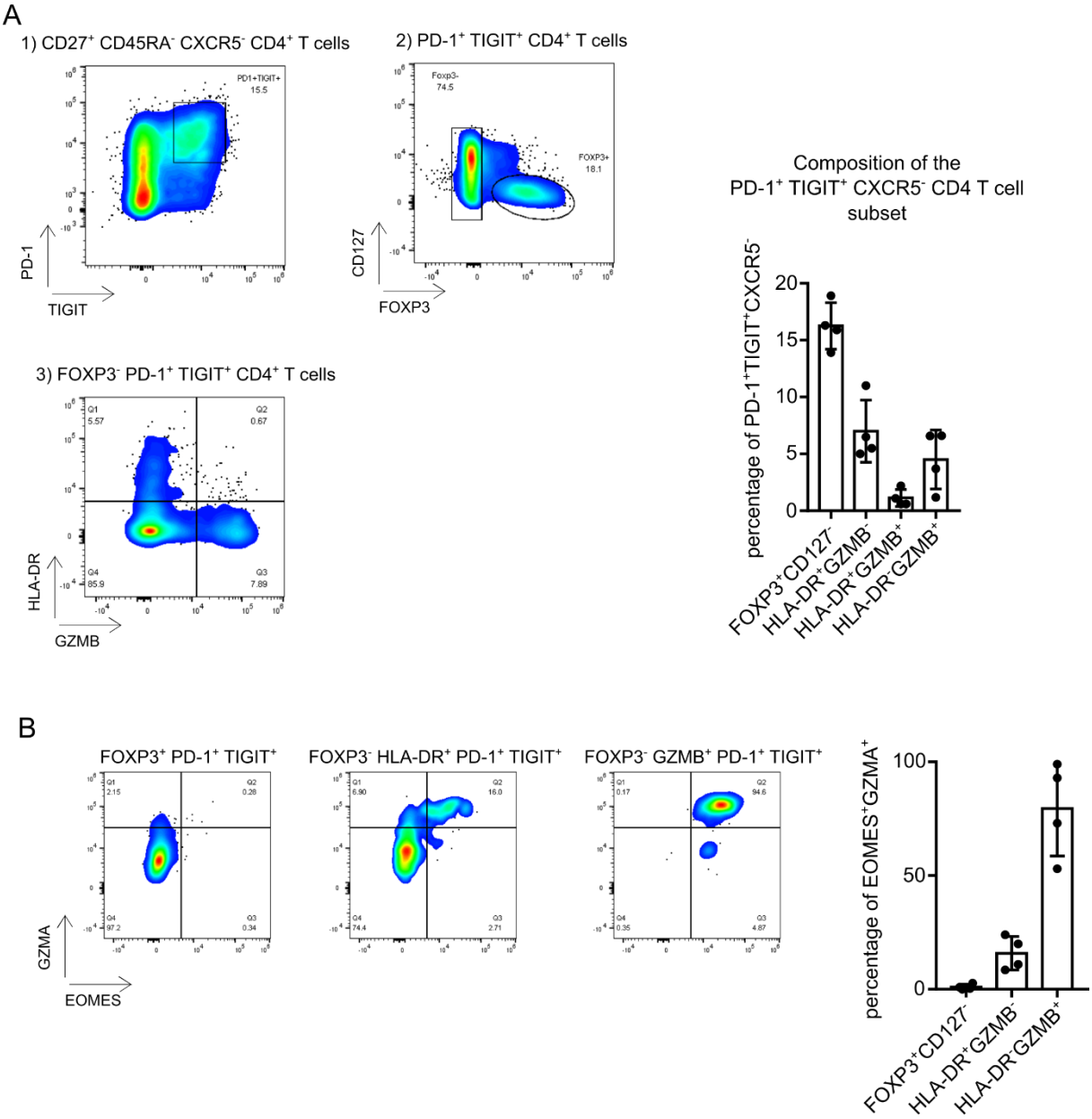

Supplementary figure 9: Intracellular characteristics of PD-1$^+$ CXCR5$^-$ TIGIT$^+$ memory CD4 T cells. (A) Foxp3, Granzyme B (GZMB) and HLA-DR expression within PD-1$^+$ CXCR5$^-$ TIGIT$^+$ memory CD4 T cells. (B) Eomes and GZMA expression by PD-1$^+$ CXCR5$^-$ TIGIT$^+$ FOXP3$^+$ (FOXP3$^+$ CD127$^-$); PD-1$^+$ CXCR5$^-$ TIGIT$^+$ FOXP3$^-$ HLA-DR$^+$ (HLA-DR$^+$ GZMB$^-$) and PD-1$^+$ CXCR5$^-$ TIGIT$^+$ GZMB+ memory CD4 T cells (HLA-DR$^-$ GZMB$^+$).

We performed a spatial multi-phenotyping analysis on a liver biopsy from one AIH patient, and we identified tertiary lymphoid structures characterized by the presence of B-cells (CD20$^+$ cells) and follicular dendritic cells (FDC, CD21$^+$) (Figure 5G, and Supplementary Figure 10). Interestingly, PD-1$^+$ CD4 T cells were enriched in the FDC and B cell zones, in comparison to the CD8$^+$ and the PD-1$^-$ CD4 T cells (Figure 5H and I, Supplementary Figure 10). The FDC area was enriched in CXCR5$^+$ cells suggesting germinal center formation and/or B cell retention (Figure 5I). Although the phenotype of the PD-1$^+$

374 $CD4^+$ T cells was less detailed, this localization suggested that liver-autoreactive CD4 T cells could be
375 involved in the B-cell response within the liver.

A

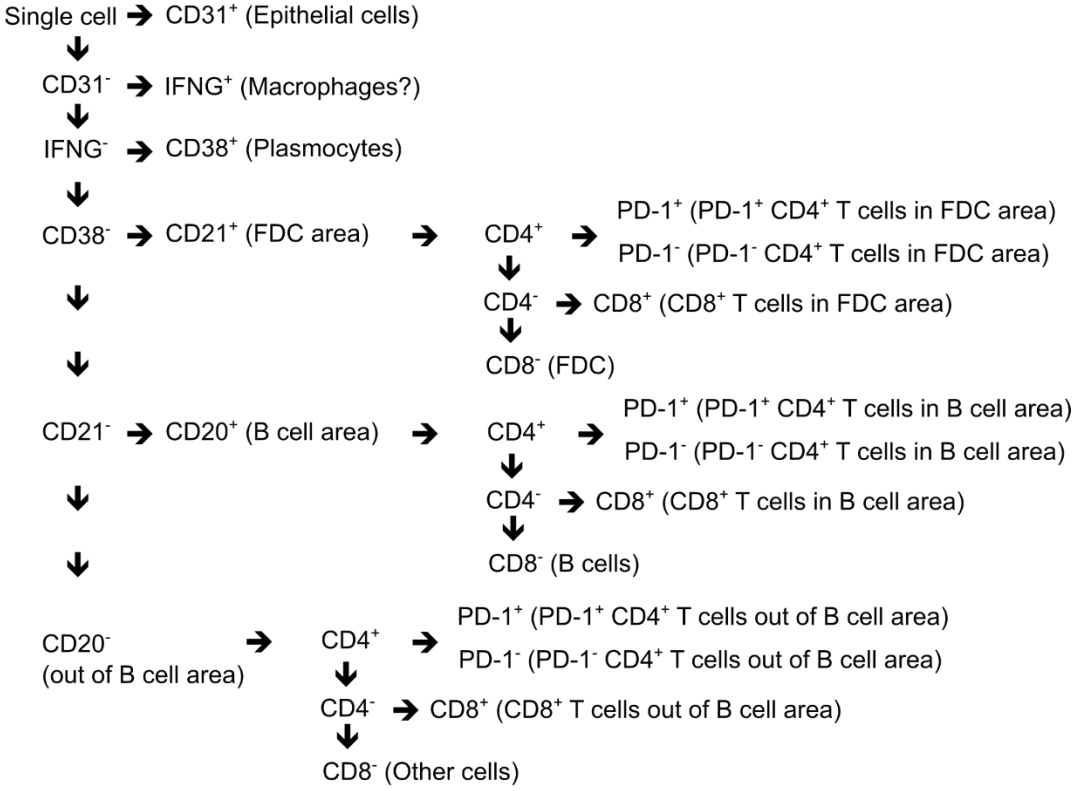
Single cell → CD31+ (Epithelial cells)
CD31- → IFNG+ (Macrophages?)
IFNG- → CD38+ (Plasmocytes)
CD38- → CD21+ (FDC area) → CD4+ → PD-1+ (PD-1+ CD4+ T cells in FDC area)
PD-1- (PD-1- CD4+ T cells in FDC area)
CD4- → CD8+ (CD8+ T cells in FDC area)
CD8- (FDC)
CD21- → CD20+ (B cell area) → CD4+ → PD-1+ (PD-1+ CD4+ T cells in B cell area)
PD-1- (PD-1- CD4+ T cells in B cell area)
CD4- → CD8+ (CD8+ T cells in B cell area)
CD8- (B cells)
CD20-
(out of B cell area) → CD4+ → PD-1+ (PD-1+ CD4+ T cells out of B cell area)
PD-1- (PD-1- CD4+ T cells out of B cell area)
CD4- → CD8+ (CD8+ T cells out of B cell area)
CD8- (Other cells)

B

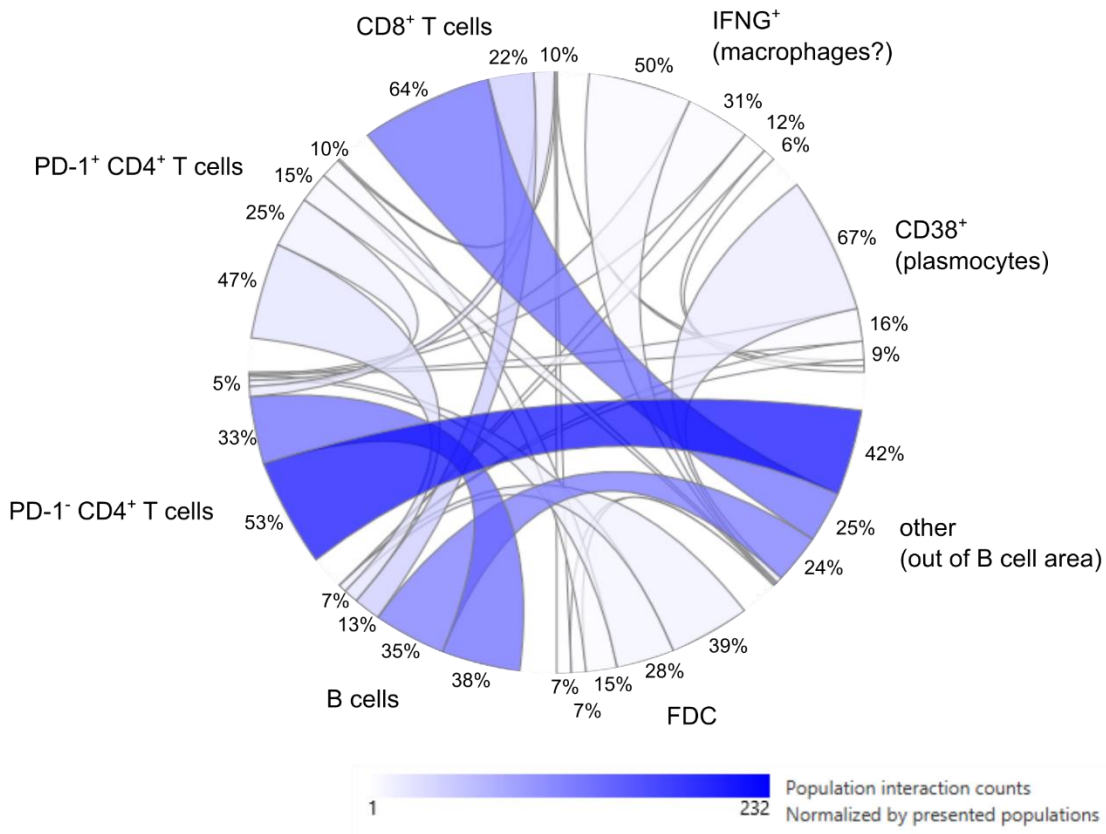
CD8+ T cells
IFNG+
(macrophages?)
CD38+
(plasmocytes)
other
(out of B cell area)
FDC
B cells
PD-1- CD4+ T cells
PD-1+ CD4+ T cells
22%
10%
50%
64%
31%
12%
6%
10%
15%
25%
67%
47%
16%
9%
5%
33%
42%
53%
25%
24%
7%
13%
35%
39%
38%
28%
7%
15%
7%
1
232
Population interaction counts
Normalized by presented populations

377 **Supplementary figure 10: Spatial lineage assignment strategy and proximity analysis.** (A) Schematic lineage assignment
378 strategy. (B) Proximity analysis between major cellular subsets identified. Analysis performs with the Multiple Analysis Viewer
379 (MAV) software.

380 ***The transcriptomic signature of liver-autoreactive CD4 T cells is dictated by the hepatic environment***

381 Since circulating liver-autoreactive CD4 T cells have a specific transcriptomic signature in humans, we
382 investigated whether their molecular profile was due to antigen reactivity in the hepatic environment
383 or to a lineage-specific signature. To answer this question, we designed a non-TCR-transgenic mouse
384 model that allows the analysis of the emergence and modulation of CD4 T cell responses against a
385 model antigen expressed by hepatocytes. We used a model of Balb/c mice in which the hemagglutinin
386 (HA) expression was restricted to hepatocytes, by an inducible Cre recombinase under the control of
387 hepatocyte-specific mTTR (transthyretin) promotor (HA/iCre) (Figure 6A and Supplementary Figure
388 11). Tamoxifen induced HA expression in the liver of HA/iCre mice but did not induce an anti-HA
389 humoral response (Figures 6A-C). Intramuscular injection of a Cre-coding adenovirus (AdCre) or an HA-
390 coding plasmid was performed to generate peripheral immunization against the HA antigen (HA i.m,
391 Figure 6A and C). HA-specific memory ($CD44^{high}$) CD4 T cells were detected with pMHCII tetramer in
392 the spleen but not in the liver of mice after peripheral immunization.

393 To analyze HA-specific CD4 T cells in the liver, we induced HA expression in the liver, by using tamoxifen
394 in pre-immunized HA/iCre mice (HA i.m + Tamoxifen, Figure 6A); we used littermates lacking liver-
395 restricted expression of an inducible Cre recombinase (Ctrl) as controls (Supplementary Figure 11). In
396 this condition, we detected HA-specific CD4 T cells in the liver of immunized mice expressing HA by
397 hepatocytes after tamoxifen treatment (Figure 6D), showing active recruitment from the periphery of
398 HA-specific memory CD4 T cells into the liver following local antigen expression. Liver HA-specific CD4
399 T cells expressed high levels of PD-1 (Figure 6E).

400 In this mouse model, we analyzed the transcriptomic profile of HA-specific CD4 T cells in mouse liver
401 and spleen. Overall, all spleen HA-specific CD4 T cells, irrespective of liver HA expression, clustered
402 together, whereas liver HA-specific CD4 T cells show a distinct transcriptomic signature (Figure 6F and
403 G). Besides expressing genes associated with the inflammatory response (e.g. *Ox40*, *Cd137*, *Ccl5* and
404 *Icos*), liver HA-specific CD4 T cells expressed genes involved in the regulation of proliferation and
405 activation (e.g. *Tigit*, *Ctla4*, *Prdm1* and *Casp3*) (Figures 6H). Comparative analysis with human liver-
406 self-antigen specific transcriptomic signature revealed four common pathways linked to the regulation
407 of T cell activation (GO:0042110 T cell activation; GO:0002694 reg. of leukocyte activation;
408 GO:0051249 reg. of lymphocyte activation; GO:0050863 reg. of T cell activation). The analysis of the
409 genes from these pathways revealed common genes shared between liver HA-specific CD4 T cells in
410 mice and circulating liver-autoreactive CD4 T cells in human (Figure 6I). Both cell types expressed high

411 levels of *TIGIT*, *CTLA-4, BATF* and *PRDM1* gene expression. These data demonstrate immuno-
412 regulatory genes were induced during local immune response in the liver. These suggest that the
413 immune signature of human circulating liver-autoreactive CD4 T cells is an imprint of the hepatic
414 environment, and could suggest that these cells leak out of damaged tissue after a phase of high
415 reactivity in the tissue.

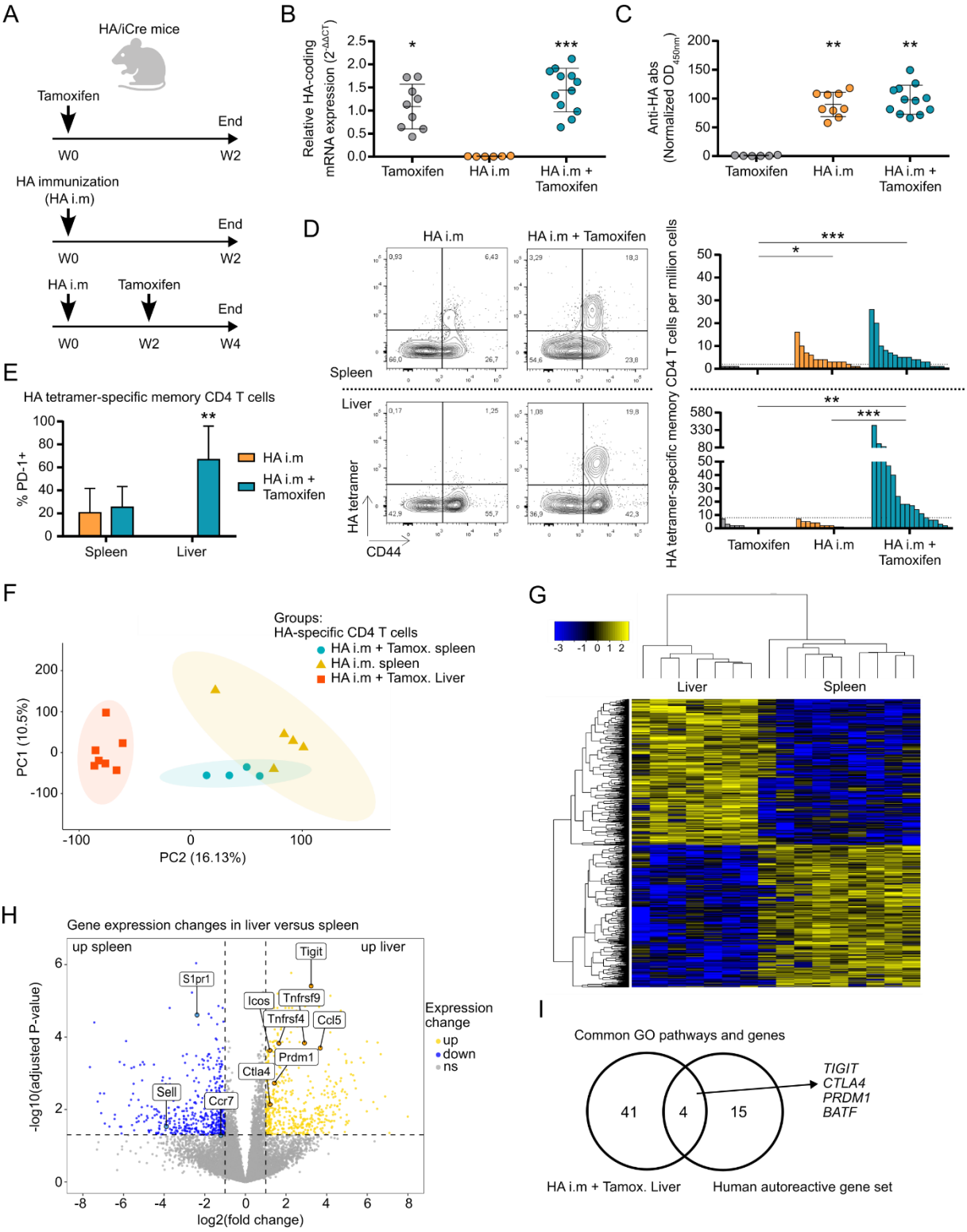

416

Figure 6: Analysis of antigen-specific CD4 T cells from the liver and the spleen of an in vivo non-TCR-transgenic mouse model. (A) Experimental design for investigation of immune response against the HA antigen in the liver. HA/iCre mice received either tamoxifen treatment (n=9), HA immunization treatment (HA i.m; n=15), or HA immunization followed 2 weeks later by tamoxifen treatment (HA i.m + Tamoxifen; n=12). Mice were euthanized 2 weeks after the last treatment. (B) Relative HA mRNA expression in the liver. ACTB was used as loading control. (C) Analysis of normalized anti-HA antibody rate in serum of mice. (D) Analysis of HA-tetramer-specific CD4 T cells in the spleen (top) and in the liver (bottom). Contour plot representation of HA tetramer staining and CD44 expression in CD4 T cells from HA i.m and HA i.m + Tamoxifen mice (left). Frequency of HA-tetramer-specific memory ($CD44^{high}$) CD4 T cells per million cells (right). Dotted lines in the frequency graphs represent threshold of positive detection of HA-specific CD4 T cell population. (E) Analysis of PD-1 expression in detectable HA-specific memory CD4 T cells from the spleen and the liver of HA i.m and HA i.m + Tamoxifen mice. (F) Principal component analysis (PCA) of bulk-RNA-seq transcriptome of HA-specific CD4 T cells isolated from the liver or the spleen. (G) Gene expression heatmap of HA-specific CD4 T cells. (H) Volcano plot of gene expression change between liver and spleen HA-specific CD4 T cells. (I) Genes from GO enrichment pathways upregulated and shared between mouse liver HA-specific CD4 T cells and human autoreactive CD4 T cells. Dunn's multiple comparisons test was used for B, C and D. Mann-Whitney test was used for E. *: p<0.05; **: p<0.01; ***: p<0.001.

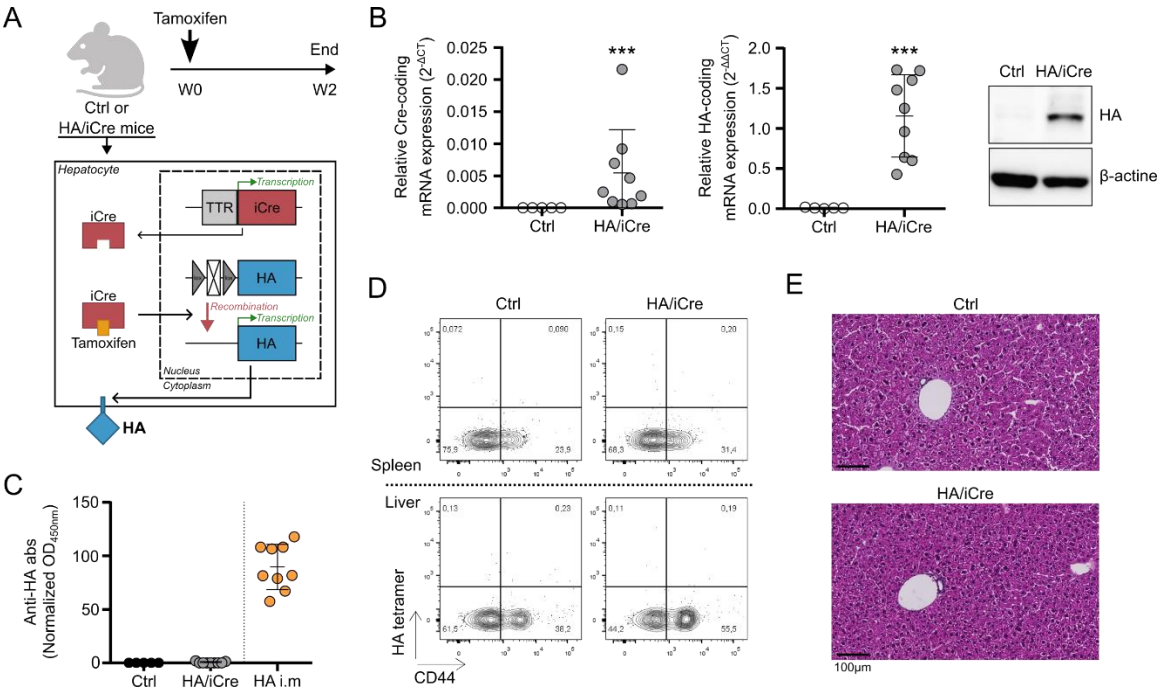

Supplementary Figure 11: Tamoxifen treatment in non-TCR-transgenic mouse model. (A) Experimental design and schematic illustration for tamoxifen treatment in Rosa26 HA floxed mice (Ctrl) and Rosa26 HA floxed TTR-inducible Cre mice (HA/iCre). (B) Relative Cre mRNA expression (left) and relative HA mRNA expression (middle) in the liver. HA protein detection from total protein extract of liver samples (left). β-actin was used as loading control. (C) Analysis of normalized anti-HA antibody rate in serum of tamoxifen-treated Ctrl and HA/iCre mice. Anti-HA antibody rate of immunized mice (HA i.m) was indicated as positive control. (D) Contour plot representation of HA tetramer staining and CD44 expression in CD4 T cells from spleen (top) and liver (bottom) of tamoxifen-treated Ctrl and HA/iCre mice. (E) Representative pictures of paraffin-embedded liver sections stained with HPS coloration. Black line is used as scale. Mann-Whitney test was used for B. ***: p<0.001.

442 ***Immune checkpoint molecules control the antigen-specific hepatitis in a CD4 T cell dependent***
443 ***manner***

444 The upregulation of immune checkpoint molecules by the antigen-specific CD4 T cells after their
445 reactivity in the liver suggested the potential regulation of these cells by the hepatic environment.
446 Therefore, we blocked PD-1 and CTLA-4 pathways, with specific antibodies as immune checkpoint
447 inhibitors (ICI), in our mouse model of hepatic infiltration by HA-specific CD4 T cells, after immunization
448 and induction of HA expression by hepatocytes (Figure 7A). The obtained data revealed a significant
449 hepatitis marked by high histological liver inflammation score when mice receiving ICI were pre-
450 immunized and expressed HA in the liver (HA/iCre + ICI, Figures 7B and C). Mice immunized but unable
451 to express HA in their liver after tamoxifen treatment did not show significant liver inflammation after
452 PD-1 and CTLA-4 blockade (Ctrl + ICI, Figures 7B and C). These data demonstrate that the hepatic
453 environment specifically regulates the antigen-specific response by engaging immune checkpoint
454 receptors.

455 Then, we assessed the role of CD4 T cells in this response by depleting $CD4^+$ cells with anti-CD4
456 antibodies in immunized HA/iCre mice treated with tamoxifen and PD-1/CTLA-4 blocking antibodies
457 (Figure 7D). First, CD4 depletion was associated with significantly lower immunization rate according
458 to anti-HA antibody levels in the serum (Figure 7E). Interestingly, histological analysis revealed
459 significantly reduced liver damages in CD4 depleted mice, showing major role of CD4 T cells in
460 promoting antigen-specific liver inflammation in our model (Figures 7F and G). The hepatic
461 inflammation observed after PD-1 and CTLA-4 blockade was linked to substantial HA-specific CD8
462 response in the spleen and in the liver, but depletion of CD4 T cells before the induction of HA
463 expression in the liver abrogated the HA-specific CD8 response (Figure 7H). These results demonstrate
464 that the hepatic environment quickly regulates local immune response against an antigen expressed
465 by hepatocytes through upregulation of immune checkpoint pathways in a CD4-dependent manner.
466 This data reveal a major role of the liver-antigen-specific CD4 T cells in the initiation of immune
467 response against a hepatic antigen.

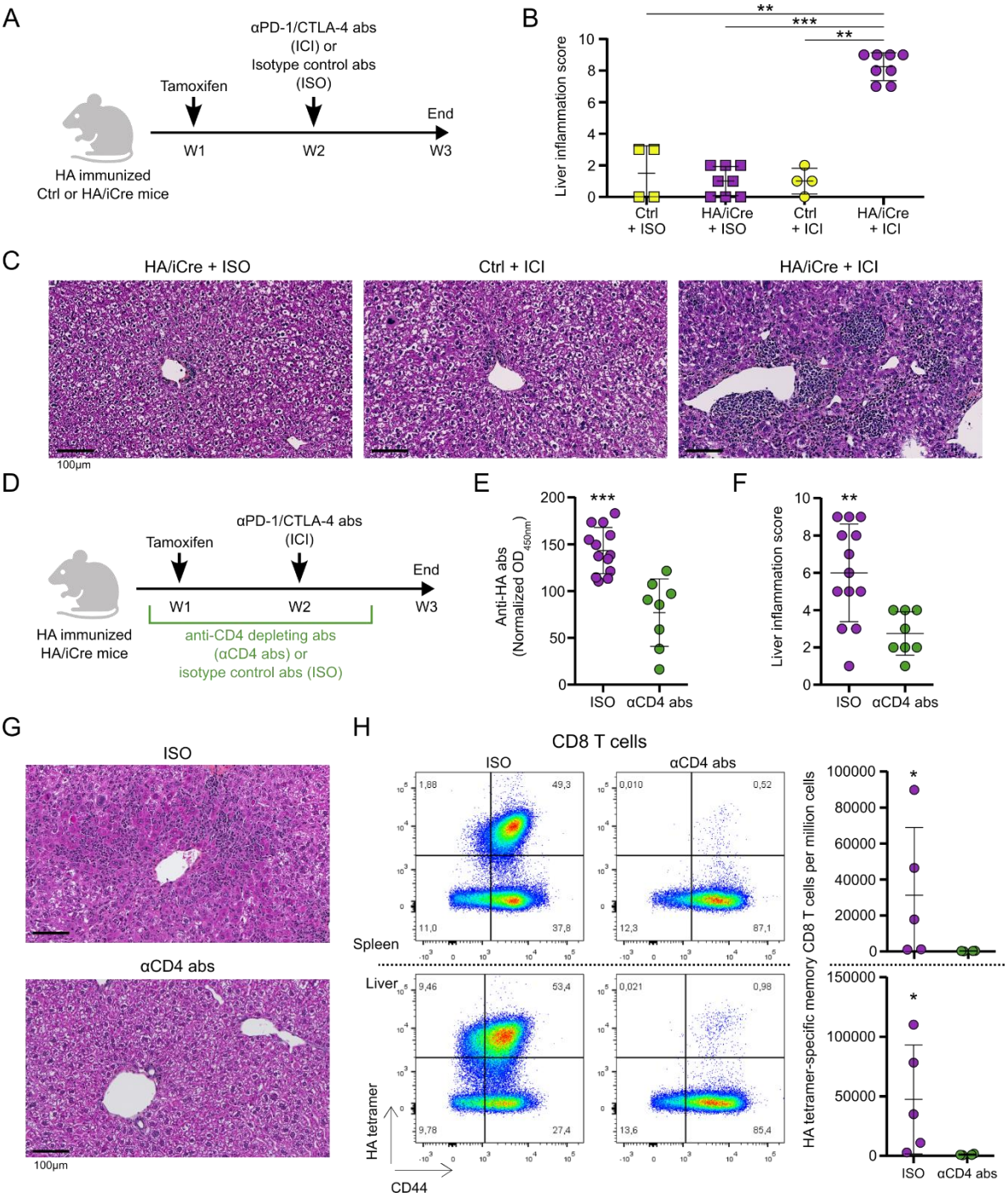

Figure 7: Immune checkpoint pathways control liver antigen-specific CD4 T cell responses and mediate hepatic tolerance. (A) Experimental design for PD-1 and CTLA-4 blockade (ICI) in HA immunized tamoxifen-treated HA/iCre mice. Injection of isotype control antibodies to ICI was used as control (ISO). (B) Histological liver inflammation scoring analysis of liver tissue sections from immunized tamoxifen-treated control (Ctrl; n=8) and HA/iCre (n=16) mice treated either with isotype control antibodies (+ ISO; Ctrl: n=4, HA/iCre: n=8) or anti-PD-1 and anti-CTLA-4 blocking antibodies (+ ICI; Ctrl: n=4, HA/iCre: n=8). (C) Representative pictures of paraffin-embedded liver sections stained with HPS coloration from indicated conditions. Black line is used as scale. (D) Experimental design for CD4 depletion (αCD4 abs) in immunized tamoxifen-treated HA/iCre mice receiving PD-1 and CTLA-4 blockade protocol (n=13). Injection of isotype control antibody to αCD4 abs was used as control (ISO; n=8). (E) Analysis of normalized anti-HA antibody rate in serum of mice. (F) Histological liver inflammation scoring analysis of liver tissue sections. (G) Representative pictures of paraffin-embedded liver sections stained with HPS coloration from indicated

479 conditions. Black line is used as scale. (H) Pseudocolor dot plot representation of HA tetramer staining and CD44 expression
480 in CD8 T cells from spleen (top) and liver (bottom) of ISO (n=5) and αCD4 abs (n=4) mice (left). Frequency of HA tetramer-
481 specific memory ($CD44^{high}$) CD8 T cells per million cells (right). Mann-Whitney test was used for B, E, F and H. *: $p<0.05$; **:
482 $p<0.01$; ***: $p<0.001$.

483 **Discussion**

484 In this study, we analyzed the transcriptome, TCR repertoire and single-cell protein expression of
485 circulating liver-self-antigen-specific CD4 T cells and expanded intrahepatic CD4 T cell clonotypes found
486 in the blood of AILD patients. We have identified a peripheral subset of liver-autoreactive CD4 T cells
487 (non-T_{REG} T_{CM} $CXCR5^-$ $CD49d^+$ $PD\text{-}1^+$ $TIGIT^+$ $ICOS^+$ $HLA\text{-}DR^+$ $CD38^+$ CD4 T cells) with an autoimmune
488 transcriptomic profile (*CXCL13, IL21, TIGIT, CTLA4, PRDM1*, *TOX, HLA-DR, CCR2, ENTPD1, LGALS1,*
489 *CXCR3, CXCR6, TIM3*) that is linked to clonal expansion in the liver. Using a mouse model to track the
490 early immune response against an antigen conditionally overexpressed in the liver, we observed that
491 liver CD4 T cells targeting this antigen acquired an immuno-exhausted (*TIGIT, PRDM1, CTLA-4)*
492 transcriptomic signature comparable to that of circulating liver-autoreactive CD4 T cells in AILD
493 patients, and are essential for inducing a complete immune response against a liver antigen
494 responsible for liver damage. Our data support the idea that circulating CD4 T cells targeting hepatic
495 antigens are liver-derived autoreactive CD4 T cells and that their transcriptomic signature is imprinted
496 by antigen encounter in the tissue. The ability to identify a subset of T cells linked to tissue auto-
497 reactivity in blood opens important prospects for the development of biomarkers and therapies. This
498 is in line with the capacity to identify tumor-specific CD8 T cells in blood which shares similarities with
499 their counterparts in tissues, and could therefore be an alternative source for identifying antitumor T
500 cell reactivity[37].

501 This study also represents the first complete deep phenotyping and transcriptome analysis of CD4 T
502 cells targeting hepatic autoantigens in human AILD. We analyzed the transcriptomic signature of the
503 CD4 T cell reactivity against three distinct liver-self-antigens and against three common foreign
504 antigens. Upon *in vitro* peptide stimulation, autoreactive CD4 T cells present a common transcriptomic
505 signature although the three self-antigens have no molecular similarity (Sepsecs, CYP2D6 and PDCE2).
506 Interestingly, this transcriptomic signature is distinct from the anti-fungus Th17 (Candida Albicans
507 reactivity) and the anti-viral (influenza H1N1 and Sars-CoV-2) immune signatures. In a previous
508 publication, we had shown that Sepsecs-specific CD4 T cells, versus CD4 T cells reactive against the
509 Candida Albicans, have a B-helper / pro-inflammatory immune signature[22]. In this new study, we
510 reinforce the data, and we demonstrate that the immune signature of liver-autoimmunity is clearly
511 distinct from diverse foreign antigen immune responses. The major immune genes characterizing this
512 signature are *TIGIT, CTLA4, NR3C1, TOX, CXCL13, STAT3,* and *PRDM1*. This autoreactive signature

513 shares a high similarity with the published signature of the T_{PH} CD4 cell subset described in the tissue
514 of other autoimmune diseases, [23,24,29,38]. However, the lack of data available at the single-cell level for
515 other self-antigen-specific CD4 T cells after short peptide stimulation makes it difficult to identify genes
516 specifically linked to hepatic autoimmunity in our dataset.

517 Interestingly, circulating liver-autoreactive CD4 T cells have a profile similar to that of tissue-infiltrating
518 CD4 T cells found in various immune contexts. Expression of PD-1, CXCL13, IL21, TIGIT, PRDM1, TOX,
519 CD39, TIM3, CTLA-4, CXCR3, CCR2, HLA-DR and CXCR6 is commonly shared with the signature of T_{PH}
520 CD4 cells in the synovium of RA patients, neoantigen-reactive CD4 T cells in metastatic human cancers,
521 tumor-infiltrating CD4 T cells, liver-infiltrating CD4 T cells in HBV-infected patients and liver-resident
522 CD4 T cells[23,39–46]. The main difference is that circulating liver-autoreactive CD4 T cells do not express
523 CD69, which is probably downregulated after tissue egress. This supports the idea that local antigenic
524 reactivity induces a significant modification of CD4 T cells, characterized by the induction of the
525 expression of immune checkpoint molecules and other. These markers found in the peripheral blood
526 may be useful for designing biomarkers related to tissue aggression. Their presence in the blood
527 stream can be explained by the fact that during the active phase of the disease, the high clonal
528 expansion in the liver may favor the recirculation of autoreactive T cells. This concept is supported by
529 the fact that the frequency of liver-autoreactive CD4 T cells in the blood of patients decreases during
530 the remission phase, which is generally associated with a reduction in intrahepatic lymphocyte activity.

531 The most common feature shared between liver-autoreactive CD4 T cells and tissue infiltrating CD4 T
532 cells is their high expression of immune-regulatory molecules (e.g. PD-1, TIGIT, CTLA-4), which may be
533 linked to local chronic antigen stimulation and exhaustion. During cancer, the blockade of PD-1 can
534 restore the activity of tumor-infiltrating CD4 T cells demonstrating their local immune involvement and
535 that immune checkpoint molecules control local reactivity[41,43]. In our study, we demonstrate that
536 immune checkpoint molecules in the liver participate in the local control of antigen-specific liver
537 damages which is dependent of the CD4 T cell response. In human, hepatic lesions can be induced by
538 anti-cancer immunotherapy (anti-PD-1 and anti-CTLA-4) and are associated with a predominant CD8 T
539 cell infiltrate in the lobular zone, suggesting a reactivation of the local liver-antigen-specific T cell
540 response[47–49]. The major difference with AIH is that during immunotherapy-induced acute hepatitis,
541 no signs of chronicity are reported, and the acute hepatitis is rapidly controlled by immunosuppressive
542 treatments without relapse after treatment withdrawal. In contrast, AIH patients' liver biopsies show
543 the complete architecture of a chronic adaptive immune response at diagnosis, which is usually late in
544 the course of the disease. A large number of B cells and of CD4 T cells are observed in the portal
545 zone[48,49]. The detection of tertiary lymphoid structures in the portal zone in our study supports the
546 idea of a prolonged activation period to achieve such immune organization.

547 These differences between acute and chronic hepatitis suggest a possible gradual escape from
548 standard immuno-regulatory processes of the liver-self-antigen-specific T cells during AILD. Studies
549 have shown links between CTLA-4 polymorphisms and susceptibility to AIH and PBC[50–55]. However, the
550 functional biological link with the development of AILD is not known. We can hypothesize that a
551 dysregulation of this pathway participates in the gradual temporal escape of liver-antigen-specific CD4
552 T cell response that mediates the expansion of cytotoxic CD8 T cells. This hypothesis may be supported
553 by the fact that we were able to detect persistent self-antigen-specific CD4 T cell clones for three years,
554 suggesting maintenance of clonal expansion. Therefore, understanding the link between genetic risk
555 and the functional capacity of autoreactive T cells to escape tolerance may open new therapeutic
556 prospects.

557 **Methods:**

558 ***Patients***

559 All the patients eligible signed a written informed consent prior to inclusion into a bio-bank of samples
560 of AILD patients (BIO-MAI-FOIE) maintained in Nantes University Hospital which obtained regulatory
561 clearance from the biomedical research Ethics Committee (CPP) and all required French Research
562 Ministries authorizations to collect biological samples (ref MESR DC-2017-2987). The biobank is
563 supported by the HEPATIMGO network promoted since 2017 (RC17_0228) by Nantes University
564 Hospital and is a prospective multi-centric collection managed by the Biological Resource center of the
565 CHU of Nantes. All data collected were treated confidentially and participants are free to withdraw
566 from the study at any time, without explanation and without prejudice to their future care. It was
567 granted authorization from the CNIL: 2001209v0). All AIH patients included in this study had a
568 simplified diagnostic score superior or equal to 6 according to the simplified scoring system for AIH of
569 the international autoimmune hepatitis group (IAHG)[5,56]. PBC patients included in this study were
570 diagnose based on cholestasis, increase serum IgM and presence of anti-mitochondria M2 (anti-M2)
571 antibody[7]. Active AIH (AIHa) patients are untreated patients with new onset AIH patients enrolled at
572 diagnosis prior any treatment initiation as previously described[57], and AIH patients under standard
573 treatment but do not normalize the transaminases (AST and ALT) and/or the serum IgG levels or are
574 under relapsing event. Remission AIH (AIHr) patients are defined biochemically by a normalization of
575 the transaminases and the IgG levels, according to the most recent European clinical practice
576 guidelines on AIH [5]. All NASH (non-Alcoholic SteatoHepatitis) patients had histological evidence of
577 NASH and had dysmetabolic syndromes. This study was carried out in accordance with the Principles
578 of International Conference on Harmonisation (ICH) Good Clinical Practice (GCP) (as adopted in France)
579 which builds upon the ethical codes contained in the current version of the Declaration of Helsinki, the

580 rules and recommendations of good international (ICH) and French clinical practice (good clinical
581 practice guidelines for biomedical research on medicinal products for human use) and the European
582 regulations and/or national legislation and regulations on clinical trials.

583 ***Peptide re-stimulation assay***

584 10 to 20x10^6 PBMCs (at a final concentration of 10x10^6/mL) were stimulated for 3 to 4h at 37°C with
585 1µg/mL of synthesized peptides spanning all of the Sepsecs, CYP2D6 or PDCE2 sequences (20 amino
586 acids in length with a 12 amino acid overlap; Synpeptide, China) or with 1µg/mL of PepTivator^R C.
587 albicans MP65, Influenza A (H1N1) MP1 and SARS-CoV-2 Prot_S (SPIKE) (peptides pools of 15 amino
588 acids length with 11 amino acid overlap, Miltenyi Biotec) in 5% human serum RPMI medium in the
589 presence of 1µg/ml anti-CD40 (HB14, Miltenyi Biotec). After 4 hrs of specific peptide stimulation,
590 PBMCs were first labeled with PE-conjugated anti-CD154 (5C8, Miltenyi Biotec) and CD154$^+$ cells were
591 then enriched using anti-PE magnetic beads (Miltenyi Biotec). A 1/10th fraction of non-enriched cells
592 was saved for frequency determination. Frequency was calculated with the formula F = n/N, where n
593 is the number of CD154 positive cells in the bound fraction after enrichment and N is the total number
594 of CD4$^+$ T cells (calculated as 10 × the number of CD4$^+$ T cells in 1/10th non-enriched fraction that was
595 saved for analysis). After enrichment, cells were stained with appropriate antibodies (Supplementary
596 table 1).

597 ***Tetramer staining***

598 For tetramer staining, 30 million PBMCs in 200 µL of 5% human serum RPMI medium were stained
599 with 20 µg/mL PE-labeled tetramers at room temperature for 100 minutes. Cells were washed and
600 incubated with anti-PE magnetic beads (Miltenyi Biotec, Germany), and a one-tenth fraction was saved
601 for analysis. The other fraction was passed through a magnetic column (Miltenyi Biotec). After
602 enrichment, cells were stained with appropriate antibodies (Supplementary table 1). $Sepsecs_{187-197}$
603 HLA-DRB1 03:01 tetramer was generated by the tetramer core at the Benaroya research institute
604 (Seattle, USA).

605 ***Flow cytometry and cell sorting***

606 All antibodies used are described in the supplementary table 1. Briefly, for surface staining, PBMCs
607 were incubated 20 minutes with a mix of antibodies and then washed prior analysis or cell sorting on
608 BD FACSCantoII, Cytek Aurora or BD FACSAriaII. For intra-cellular staining we used the
609 Fixation/Permeabilization Solution Kit (BD Cytofix/Cytoperm™, BD Biosciences).

610 ***Single cell RNA sequencing and analysis (plate-based assays)***

611 For scRNA-seq analysis of peptide-restimulated CD4 T cells, CD154^{+} memory CD4 T cells were first
612 sorted on BD FACSAriaII, one cell per well, in 96-well plates containing specific lysis buffer at the CRTI,
613 Nantes. Plates were immediately frozen for storage at -80°C, and sent on dry ice to the Genomics core
614 facility of CIML, Marseille, for further generating scRNAseq libraries with the FB5P-seq protocol as
615 described[22,58]. Briefly, mRNA reverse transcription (RT), cDNA 5'-end barcoding and PCR amplification
616 were performed with a template switching (TS) approach. After amplification, barcoded full-length
617 cDNA from each well were pooled for purification and library preparation. For each plate, an Illumina
618 sequencing library targeting the 5'-end of barcoded cDNA was prepared by a modified transposase-
619 based method incorporating a plate-associated i7 barcode. Resulting libraries had a broad size
620 distribution, resulting in gene template reads covering the 5'-end of transcripts from the 3rd to the 60th
621 percentile of gene body length on average. As a consequence, sequencing reads covered the whole
622 variable and a significant portion of the constant region of the TCRα and TCRβ expressed mRNAs,
623 enabling assembly and reconstitution of TCR repertoire from scRNAseq data. Libraries prepared with
624 the FB5P-seq protocol were sequenced on Illumina NextSeq2000 platform with P2 100-cycle kits,
625 targeting $5x10^5$-$1x10^6$ reads per cell in paired-end single-index mode with the following configuration:
626 Read1 (gene template) 103 cycles, Read i7 (plate barcode) 8 cycles, Read2 (cell barcode and Unique
627 Molecular Identifier) 16 cycles. We then used a custom bioinformatics pipeline to process fastq files
628 and generate single-cell gene expression matrices and TCR sequence files, as described[22,58].

629 For scRNA-seq of tetramer-stained CD4 T cells, we used an updated version of FB5P-seq (Flash-FB5P-
630 seq) modified to implement advances developed by Hahaut et al. in the Flash-seq protocol[59]. Cells were
631 sorted in 2 µl lysis mix composed of 0.1% Triton X-100 (0.02 µl), 1.2 U/µl recombinant RNAse inhibitor
632 (0.06 µl), 6 mM dNTP mix (0.48 µl), 1.6 mM RT primer (5'-
633 TGCGGTATCTAAAGCGGTGAGTTTTTTTTTTTTTTTTTTTTTTTTTTTTT*V*N-3') (0.36 µl), 0.0125 pg/µl
634 ERCC spike-in mix (0.05 µl), 9 mM dCTP (0.18 µl), 1 M betaine (0.4 µl), 1.2 mM DTT (0.024 µl) and PCR-
635 grade H_2O (0.426 µl). Plates were conserved at -80°C until sorting, thawed at RT for cell sorting, and
636 immediately refrozen on dry ice then conserved at -80°C until further processing. Reverse transcription
637 with template switching and cDNA amplification were performed in a single step. Each plate containing
638 cells in lysis mix was thawed on ice, heated at 72°C for 3 min then immediately placed on ice. To each
639 well containing 2 µl cell lysate, we added 8 µl of an RT-PCR mix composed of 2 U/µl Superscript IV
640 reverse transcriptase (0.1 µl), 0.8 U/µl recombinant RNAse inhibitor (0.2 µl), 1X KAPA HiFi ReadyMix (5
641 µl), 4.8 mM DTT (0.48 µl), 0.8 M betaine (1.6 µl), 9.2 mM $MgCl_2$ (0.092 µl), 0.1 µM forward PCR primer
642 (5'-AGACGTGTGCTCTTCCGAT*C*T-3') (0.1 µl), 0.1 µM reverse PCR primer (5'-
643 TGCGGTATCTAAAGCGGTG*A*G-3') (0.1 µl), 1.84 µM biotinylated barcoding template switching
644 oligonucleotide (5'-biotin-AGACGTGTGCTCTTCCGATCTXXXXXXXXNNNNNNNNCAGCArGrGrG-3', where

645 XXXXXXXX are well-specific barcodes as published[58], NNNNNNNN are random nucleotides serving as
646 Unique Molecular Identifiers, and rG are riboguanosine RNA bases) (0.184 µl) and PCR-grade H_2O
647 (0.144 µl). Then plates were incubated in a thermal cycler 60 min at 50°C, 3 min at 98°C, and 22 cycles
648 of 20 sec at 98°C, 20 sec at 67°C and 6 min at 72°C. We then pooled 5 µl amplified cDNA from all wells
649 into one tube per plate, and performed 0.6X SPRI bead-based purification. Sequencing libraries were
650 prepared from 800 pg cDNA per plate with the Illumina Nextera XT protocol, modified to target
651 sequencing reads to the 5' end of cDNA, as described [22,58]. Before sequencing, pooled indexed libraries
652 were depleted from ribosomal RNA-derived cDNA molecules by using the SEQoia RiboDepletion Kit
653 (Biorad) according to the manufacturer's instructions. Flash-FB5P-seq libraries were sequenced on an
654 Illumina NextSeq2000 using P3 100 cycle kit and targeting $5x10^5$-$1x10^6$ reads per cell in paired-end
655 single-index mode with the following configuration: Read1 (gene template) 114 cycles, Read i7 (plate
656 barcode) 8 cycles, Read2 (cell barcode and Unique Molecular Identifier) 16 cycles. We then used a
657 custom bioinformatics pipeline to process fastq files and generate single-cell gene expression matrices
658 and TCR sequence files. Briefly, reads were processed with the zUMIs pipeline[60] to generate the gene
659 expression UMI count matrix, and with the TRUST4 pipeline[61] to reconstruct TCR sequences.

660 Quality control excluded cells with more than 10% mitochondrial UMIs, less than 400 genes, more than
661 25% ERCC UMIs, less than 0.7 ERCC spike-in quantification accuracy[58], and less than 5% ribosomal
662 protein coding UMIs. Gene expression UMI matrices were analyzed with the *Seurat v4.1.0* package in
663 R v4.1.2 using standard log normalization, 4,000 highly variable genes (computed with the *vst* method)
664 from which we removed all TCR coding genes, 40 principal components for computing UMAP and
665 Louvain clustering at resolution 0.8. Marker genes of unsupervised clusters or metadata-defined
666 clusters were computed with the *FindAllMarkers* function using Wilcoxon test with an adjusted p-value
667 cutoff of 0.01. Gene expression heatmaps were generated with the *pheatmap* function. TCR
668 clonotypes were computed and analyzed as described previously[22].

669 ***Single cell RNA sequencing and analysis (10X Genomics protocol)***

670 First, PD-1^+CD45RA^-CXCR5^- and PD-1^-CD45RA^-CXCR5^- CD4 T cells were sorted on BD FACSAriaII. Cells
671 were counted, centrifuged (500g, 5 min, 4°c) then resuspended at the recommended dilution for a
672 20000 cell loading per sample onto a Next GEM Chip K (PN-1000286) and run on a Chromium Single
673 Cell Controller using the Chromium Single Cell 5' V2 Next GEM single cell kit (PN-1000263) according
674 to the manufacturer's instructions (CG000331, 10X Genomics). Gex and VDJ-TCR libraries were then
675 prepared (PN-1000190, PN-1000252, PN-1000215 also from 10X genomics), checked for quality
676 controls and sequenced on a S2 flow cell on a Nova-Seq 6000 (Illumina) at the GenoBird platform (IRS-
677 UN, CHU Nantes). Raw reads were analyzed using FastQC for quality controls and were then processed

678 using CellRanger pipeline (v3.1.0 with default parameters). Generated FASTQ files were aligned to the
679 human reference genome GRCh38.

680 The base calling has been done using Illumina bcl2fastq2 (v2.20). The FASTQs obtained has been
681 analyzed for cell identification and UMIs count using 10X Genomics Cell Ranger 7.0.1 and hg38
682 reference. Four filtered matrices were obtained for each sample and the script written for their analysis
683 has been written in R (v4.2.2). The matrices have been analyzed using Seurat 4[62] using default
684 parameters. Each matrix has been filtered with the following cut-off: 500 < Features_RNA < 4000 ;
685 percent.mt < 5 and cells having two distinct TRA and TRB identified have been removed for the rest of
686 the analysis. Then each matrix has been normalized using the SCTransform method with a regression
687 on the percentage of ribosomal genes count. The four matrices has been merged and integrated using
688 harmony package[63]. The cell clusters have been identified using harmony for reduction. The markers
689 for each clusters have been identified with a min.pct=0.25 (genes detected in a minimum fraction of
690 min.pct cells) and a threshold of logFoldChange of 0.25. The markers retained for each cluster where
691 those having a p-value adjusted < 0.01. The annotation of clusters has been done using azimuth
692 package[62]. The module score has been calculated for each cluster using a predefined list of genes for
693 "Auto-reactive", "SARS-CoV-2", "H1N1" and "C.ALB". The top five percent of cells base on this module
694 score has been highlighted on the UMAP. The clusters have been then compared based on their
695 module score for each gene list using Kruskal Wallis test followed by a paired Wilcoxon rank test.

696 ***Mini-bulk-RNA sequencing and analysis***

697 For mini-bulk RNA-seq of *in vitro* stimulated CD4 T cells, we used a slightly modified version of the
698 Flash-FB5P-seq protocol described above. First, CD4 T cell subsets were sorted on BD FACSAriaII. 500
699 to 2000 cells per well were stimulated in presence of 2.5µg/ml anti-CD3 and 1µg/ml anti-CD28. After
700 24h, cells were washed gently in PBS and resuspended in 4µL of specific lysis buffer with the
701 composition described above except for ERCC spike-in mix which we used 10-time more concentrated
702 (0.125 pg/µl). We performed RT-PCR with 16 µl of the RT-PCR mix described above, using 16 cycles of
703 PCR for cDNA amplification (instead of 22 cycles for single-cell assay). Sequencing libraries were
704 prepared and sequenced as described above for Flash-FB5P-seq. Sequencing reads were processed
705 with the zUMIs pipeline[60] to generate gene expression UMI count matrices. Mini-bulk gene expression
706 UMI count matrices were pooled across plates and further processed with the *DEseq2* package for
707 normalization (*vst* method) and computation of differentially expressed genes between non-
708 stimulated and TCR-stimulated cells from each sorted phenotype. The mean of normalized expression
709 values for manually selected significant DE genes was used to construct the heatmaps in Figure 5F.

710 ***Bulk TCRβ sequencing***

711 $100x10^3$ PD-1$^+$CD45RA$^-$CXCR5$^-$ and PD-1$^-$CD45RA$^-$CXCR5$^-$ CD4 T cell subsets were sorted on a BD
712 FACSAriaII. gDNA from T cells and frozen liver biopsies was extracted with NucleoSpin® Blood kit
713 (Macherey-Nagel) and TCRβ sequencing was performed as previously described[64].

714 ***Unsupervised flow cytometry analysis***

715 Flow cytometry data from patients were analyzed using Omiq software (Dotmatics, USA). Subsampling
716 of viable lymphoid CD45RA$^-$ CD4$^+$ CD3$^+$ cells was performed ($20x10^3$ per patients). Clustering was
717 performed using FlowSOM to generate 150 clusters. 22 Metacluster were generated by running
718 consensus metaclustering. Wilcoxon test was used to identify significant variation between two groups
719 of patients.

720 ***Spatial multi-phenotyping and analysis (Phenocycler instrument)***

721 The PhenoCycler™ instrument (Akoya Biosciences, USA) performs iterative annealing and removal of
722 fluorophore-conjugated oligo probes to primary antibody-conjugated complementary DNA barcodes.
723 Antibody panel was constructed using 11 ready-to-use commercially available PhenoCycler™
724 antibodies (Akoya Biosciences) and one antibody unavailable has been custom conjugated. Detailed
725 12-plex PhenoCycler™ information is provided in Supplementary table 1. Anti-CXCR5 antibody has
726 been custom conjugated with a unique PhenoCycler™ oligonucleotide tag using the antibody
727 conjugation kit of Akoya Biosciences following their instructions.

728 FFPE human liver was sectioned to a thickness of 5 µm and directly adhered onto poly-L-lysine (Sigma
729 Aldrich) coated 22 x 22 mm coverslips (Akoya Biosciences). Tissue coverslips were stored at 4°C until
730 staining. The sample was incubated for 20 minutes at 55°C on a hot plate and tissue was cooled down
731 before staining. Tissue section was deparaffinized and rehydrated by immersing the coverslip through
732 the following solution for 5 minutes each : twice in OTTIX, twice in 100% Ethanol, once in 90%, 70%,
733 50%, 30% Ethanol and twice in ddH2O. Antigen retrieval was performed in a hot water bath at 100°C
734 in a 1X Citrate Buffer (Sigma Aldrich) for 30 minutes. After cooling at room temperature, tissue section
735 was briefly washed twice in ddH2O for 2 minutes. Following hydration step, tissue section was blocked
736 in Staining buffer at room temperature for 20 minutes and stained with the 12 plex PhenoCycler™
737 antibody panel in a humidity chamber 3 hours at room temperature. To ensure that the antibodies
738 remain attached to the antigen during the multicycles PhenoCycler™ imaging, protocol post-staining
739 protocol has 3 fixing steps. After incubation with antibodies, tissue section was washed twice and post-
740 fixed with 1.6% PFA Storage buffer for 10 minutes at room temperature. Tissue sections were briefly
741 washed three times in 1X PBS buffer and incubated in a cold methanol solution for 5 minutes. Following
742 washing, tissue section was fixed in final fixative solution for 20 minutes at room temperature. Finally,

743 tissue section was washed three times in 1X PBS buffer and was stored in Storage Buffer at 4°C before
744 PhenoCycler™ imaging.

745 PhenoCycler™ imaging was performed with an Axio Observer (Zeiss) inverted microscope equipped
746 with camera ORCA Flash 4.0 LT (Hamamatsu). The microscope is coupled to the Colibri 7 LED light
747 source (Zeiss) and fluorescence was detected using the monoband filter Set 112 HE LED (Zeiss). The
748 PhenoCycler™ experimental run was managed by the instrument controller software (v1.30.0.12,
749 Akoya Biosciences) integrating with the Zeiss microscope. Nuclear DAPI staining was used to design
750 manually tiled regions of interest at the 5x magnification (N-Achro 5x/0.15 M27, Zeiss). Automated
751 multiplex imaging was performed using a Plan Apo 20x/0.8 M27 Air objective (Zeiss) with a 325 x 325
752 nm pixel size using software autofocus repeated every tile before acquiring a 11 plane-z-stack with a
753 z-spacing of 1.5 µm. Data are acquired as 3D stacks by cycle of 4 markers (including a recurrent nuclear
754 DAPI staining). After acquisition, raw files were exported using the CODEX Instrument Manager (CIM,
755 Akoya Biosciences). The data are processed by computing the more in focus image from the stack to
756 take into account the potential tissue unflatness, every cycles are registered together based on the
757 DAPI staining, and the fluorescence signal is corrected by background fluorescence based on blank
758 cycles and normalized in intensity. Cell segmentation was done by using Cellpose algorithm. After
759 segmentation, measurement data are transformed in FCS files and analyzed with the CODEX MAV
760 software.

761 ***Mice and treatments***

762 Heterozygous transthyretin (TTR)-inducible Cre (iCre) mice, originally on a C57Bl6 backgroud[65], were
763 back-crossed on a Balb/c background for at least 10 generations (TAAM, CDTA CNRS Orléans, FRANCE).
764 They were cross-bred with homozygous Rosa26 hemagglutinin (HA) floxed mice mice (Rosa26$^{tm(HA)1Libl}$,
765 Kindly provided by R. Liblau, Toulouse, France[66]), resulting in heterozygous Rosa26 HA floxed (Ctrl)
766 mice and Rosa26 HA floxed TTR-inducible Cre (HA/iCre) mice. Mice were genotyped for Cre-coding
767 gene at 3 weeks-old thanks to small tail biopsies using following Cre primers: 5'-
768 CCTGGAAAATGCTTCTGTCCG-3' sense sequence and 5'-CAGGGTGTTATAAGCAATCCC-3' antisense
769 sequence. Male and female eight to twelve-weeks-old mice were used for each experiment. All mice
770 were housed at the UTE IRS-UN animal facilities (Nantes, FRANCE) where they were fed *ad libitum* and
771 allowed continuous access to tap water. Procedures were approved by the regional ethical committee
772 for animal care and use and by the Ministère de l'enseignement supérieur et de la recherche
773 (agreements APAFIS #2054, #28582 and #43529). All experiments were performed in accordance with
774 relevant guidelines and regulations.

775 Induction of HA expression by hepatocytes was performed by feeding mice with tamoxifen dry food
776 (0.5g/kg tamoxifen + 5% saccharose; Safe, FRANCE) for 14 days in free access or by injecting
777 intraperitonially (i.p) 1mg of tamoxifen diluted in corn oil three times in two weeks span. Peripheral
778 immunization against HA was performed with two different materials: one intramuscular (i.m)
779 injection of $1,5.10^9$ infectious particle of adenoviral CAG Cre vectors (AdCre, produced by INSERM UMR
780 1089 CPV facility, Nantes, FRANCE) in *tibialis anterior* of one posterior leg or i.m injection of 50µg of
781 plasmid CMV HA vector in *tibialis anterior* of both posterior legs, twice three weeks apart.

782 Immune checkpoint blockade protocol was performed by intravenous (i.v) injection of 200µg of anti-
783 mouse PD-1 antibody (29F.1A12™ clone, BioXCell) and 200µg of anti-mouse CTLA-4 antibody (9H10
784 clone, BioXCell), using purified Rat IgG2a,κ isotype control antibody (RTK2758 clone, Biolegend) and
785 polyclonal Syrian Hamster IgG antibody (ref BE0087, BioXCell) as controls, three times in one week
786 span. Depletion of $CD4^+$ cells was performed by i.p injection of 500µg of anti-mouse CD4 antibody
787 (GK1.5 clone, BioXCell), using purified Rat IgG2b,κ isotype control antibody (LTF-2 clone, BioXCell),
788 every two days during two weeks.

789 ***RNA extraction, reverse transcription and quantitative PCR***

790 Total RNA was extracted from organ tissue using TRIzol™ reagent (15596026, ThermoFisher Scientific)
791 and purified with RNeasy Mini Kit (74106, Qiagen) according to the manufacturer protocol. Reverse
792 transcription was performed using 2µg of total RNA incubated at 70°C for 10min with poly-dT24
793 20µg/mL (Eurofins Genomics), 8mM DTT (18057018, ThermoFisher Scientific) and 20mM of each dNTP
794 (10297018, ThermoFisher Scientific). After a brief 5min incubation at 4°C, first strand buffer 5X
795 (Y00146, Invitrogen), 200U of M-MLV reverse transcriptase (18057018, ThermoFisher Scientific) and
796 40U of RNAse OUT inhibitor (10777019, Invitrogen) were added and incubated at 37°C for 1h followed
797 by 15min at 70°C. Real-time quantitative PCR was performed using the ViiA™ 7 Real-Time PCR System
798 and Power SYBR™ Green PCR Master Mix (4368708, ThermoFisher Scientific). Primers for HA (5'-
799 AAACTCTTCGCGGTCTTTCCA-3' sense sequence and 5'-GATAAGGTAGCTTGGGCTGC-3' antisense
800 sequence), Cre (see primers used for mice genotyping) and ACTB (5'-TACCACAGGCATTGTGATGG-3'
801 sense sequence and 5'-AATAGTGATGACCTGGCCGT-3' antisense sequence) were used. Relative HA
802 mRNA expression was determined with $2^{-\Delta\Delta CT}$ calculation, taking ACTB as reference gene and cDNA
803 from one conserved mouse that received i.v injection of AdCre (AdCre i.v) as positive control. Relative
804 Cre mRNA expression was determined with $2^{-\Delta CT}$ calculation, taking ACTB as reference gene.

805 ***ELISA test***

806 Blood sample clotted for 1h at room temperature followed by centrifugation at 3000g for 10min and
807 serum was harvested and stored at -80°C. For detection of anti-HA antibodies, wells were coated with

808 1µg/mL of HA protein (11684-V08H, SinoBiological) diluted in coating buffer (Na_2CO_3 0.05M; $NaHCO_3$
809 0.05M; pH 9.2) and plate was incubated at 4°C overnight. Wells were washed and saturated with
810 dilution buffer (PBS 1X; Tween 20 0.05%; BSA 1%) for 2h at 37°C. Wells were washed, serum samples
811 were diluted by 500, 1000 and 5000 and added to wells in duplicate, and plate was incubated at 37°C
812 for 2h. Wells were washed and 0,4ng/mL of detection antibody (peroxidase-conjugated goat anti-
813 mouse IgG+IgM (H+L) polyclonal antibody, 115-036-068, Jackson ImmunoResearch) was added and
814 plate was incubated at 37°C for 1h. Finally, wells were washed and 50µL of TMB Substrate Reagent
815 (555214, BD Biosciences) was added for revelation step. Reaction was stopped 1min30sec after with
816 H_2SO_4 0.5M. Optical density (OD) at 450nm and 620nm were determined using a Spark® 10M Infinite
817 M200 Pro plate reader (TECAN). Analysis was performed by subtract OD_{620nm} to OD_{450nm} value, calculate
818 the mean of each duplicate and subtract the mean of blank wells to the mean of samples. Then, OD
819 values of each dilution of sample were normalized to OD values of each corresponding dilution of
820 positive control serum sample from one conserved AdCre i.v mouse. Finally, for each sample, mean of
821 normalized OD_{450nm} for each dilution was calculated and analyzed.

822 ***Cell preparation, tetramer enrichment and staining and flow cytometry***

823 Splenocytes were isolated by mechanical dissociation of spleen in red blood cell lysis buffer (NH_4Cl
824 155mM; $KHCO_3$ 10mM; EDTA 1mM; Tris 17mM per 1L of sterilized water). Liver non-parenchymal cells
825 (NPCs) were isolated as previously described[67] from liver sample perfused with HBSS 1X. Briefly, livers
826 were digested with collagenase IV, then NPCs were enriched by Percoll density gradient centrifugation
827 and red blood cells lysis. 20.10^6 splenocytes and 3.10^6 NPCs were stained with both I-A^d-HA peptide
828 (HNTNGVTAACSHE) and I-E^d-HA peptide (SFERFEIFPKE) PE-labelled tetramers (NIH Tetramer Core
829 Facility; Atlanta, USA) at room temperature during 1h. Cells were washed and stained with magnetic
830 anti-PE microbeads (130-048-801, Miltenyi) at 4°C during 15min. Cells were washed and enriched using
831 magnetic MS columns (130-042-201, Miltenyi). Positive fraction was kept for HA-specific $CD4^+$ T cell
832 detection. Negative fraction was stained with H-$2K^d$-HA peptide (PEYWEEQTQRAKSD) PE-labelled
833 tetramer (NIH Tetramer Core Facility; Atlanta, USA) at room temperature during 1h for HA-specific
834 $CD8^+$ T cell detection. All cells were washed and viability staining (LIVE/DEAD™ Fixable Aqua Dead Cell
835 Stain kit, L34957, ThermoFisher Scientific) was performed at 4°C during 15min, protected from light.
836 Cells were washed and extracellular staining were performed at 4°C during 20min protected from light,
837 using fluorochrome-coupled anti-mouse antibodies (Supplementary table 1). Fluorescence was
838 measured on BD FACSCantoII or BD FACSAriaII (BD Biosciences; Mountain View, USA). HA-specific
839 memory CD4 (or CD8) T lymphocytes were defined as: LIVE/$DEAD^-$ $CD19^-$ $CD4^+$ (or $CD8^+$) $CD44^{high}$
840 $tetramer^+$ cells. FlowJo software (TreeStar Inc) was used to analyze flow cytometry data.

841 ***3'-end bulk RNA sequencing***

842 50 up to 200 HA-specific memory $CD4^+$ T cells were FACS sorted. RNA extraction, reverse transcription
843 and PCR steps were directly performed after sorting according to the SMART-Seq® v4 Ultra® Low Input
844 RNA Kit protocol (Takara Bio, USA). Amplified complementary DNA were transferred to the Benaroya
845 Research Institute (Seattle, USA) to perform a 3'-end bulk RNA sequencing. To normalize, trimmed-
846 mean of M values (TMM) normalization on the raw gene counts was performed. Additionally, because
847 many genes are not expressed in any of the samples and are therefore uninformative, a filtering step
848 was performed requiring that genes are expressed with at least 1 count per million total reads in at
849 least 10% of the total number of libraries. For the differential gene expression analysis, we used the
850 following threshold: fold change (FC) > 2 and adjusted p value < 0.1.

851 ***Histological analysis***

852 Liver lobes were fixed in formol 4% (VWR) for 24h at room temperature. Dehydration in differential
853 absolute ethanol baths, embedding in paraffin and staining of paraffin-embedded sections (3µm) with
854 hematoxylin-phloxin-saffron (HPS) coloration were performed by the IBISA MicroPICell facility
855 (Biogenouest; Nantes, FRANCE). Slides were scanned and observed using NanoZoomer (Hamamatsu)
856 and NDP Scan software. Histological analysis was performed thanks to a liver inflammation scoring
857 method based on established hepatitis grading[68], simplified to portal inflammation score (0 to 4),
858 lobular inflammation score (0 to 4) and presence of interface hepatitis (0 to 1), giving a minimum score
859 of 0 and maximum score of 9. Liver inflammation scoring was performed blindly.

860 ***Western blot***

861 Total proteins were extracted from liver samples via RIPA buffer treatment. 25µg of protein were
862 denatured at 95°C for 5min in Laemmli Sample Buffer (161747, Bio-Rad) with DTT 0.1M. Preparation
863 was separated by SDS-PAGE on Mini-PROTEAN TGX Precast Protein Gels (4561036, Bio-Rad) in
864 migration buffer (Tris 15g/L; Glycine 72g/L; SDS 10g/L) and transferred onto a PVDF membrane with
865 the Trans-Blot Turbo Transfer System (Bio-Rad). The membrane was blocked for 2h with a blocking
866 solution (TBS; Tween 20 0.1%; Skim milk 5%), followed by overnight incubation at 4°C with anti-HA
867 antibody (rabbit polyclonal antibody; 11684-T62, Sinobiological) and anti-mouse β-actin antibody
868 (mouse monoclonal antibody; 3700, Cell Signaling) as primary antibodies. The membrane was washed
869 and incubated 1h at room temperature with peroxidase-conjugated donkey anti-rabbit IgG (H+L)
870 antibody (E-AB-1080-120, Cliniscience) and peroxidase-conjugated goat anti-mouse IgG+IgM (H+L)
871 antibody (115-036-068, Jackson ImmunoResearch). Revelation was performed by
872 Electrochemioluminescence Super Signal West Pico (34577, ThermoFisher Scientific) according to the

873 manufacturer instructions. Imaging and analysis of western blots were performed on the ChemiDoc
874 MP Imaging System (Bio-Rad).

875 ***Statistical analysis***

876 Statistical comparisons were performed using GraphPad Prism software V.5 (GraphPad Software, La
877 Jolla, CA, USA) and FaDA[69] (https://shiny-bird.univ-nantes.fr/app/Fada). P value <0.05 after adjustment
878 were considered significant.

Name	Clone	Antigen	Brand	Reactivity	Application
APC/Cyanine7 anti-human CD69	FN50	CD69	BioLegend	Human	Flowcytometry
Alexa Fluor®647 anti-human CD185 (CXCR5)	J252D4	CD185	BioLegend	Human	Flowcytometry
PerCP/Cyanine5.5 anti-human CD279 (PD-1)	EH12.2H7	CD279	BioLegend	Human	Flowcytometry
Alexa Fluor® 488 anti-human CD4	OKT4	CD4	BioLegend	Human	Flowcytometry
APC/Cyanine7 anti-human CD4	RPA-T4	CD4	BioLegend	Human	Flowcytometry
Alexa Fluor®647 anti-human CD25	BC96	CD25	Invitrogen	Human	Flowcytometry
PerCP/Cyanine5.5 anti-human HLA-DR	G46-6	HLA-DR	BD Biosciences	Human	Flowcytometry
Alexa Fluor® 488 anti-human CD185 (CXCR5)	RF8B2	CD185	BD Biosciences	Human	Flowcytometry
Brilliant Violet 421™ anti-human CD45RA	HI100	CD45RA	BioLegend	Human	Flowcytometry
APC anti-human CD184 (CXCR4)	12G5	CD184	BioLegend	Human	Flowcytometry
Brilliant Violet 421™ anti-human CD278 (ICOS)	C398.4A	CD278	BioLegend	Human	Flowcytometry
Brilliant Violet 605™ anti-human CD200 (OX2)	OX-104	CD200	BioLegend	Human	Flowcytometry
Brilliant Violet 650™ anti-human CD183 (CXCR3)	G025H7	CD183	BioLegend	Human	Flowcytometry
Brilliant Violet 711™ anti-human CD196 (CCR6)	G034E3	CD196	BioLegend	Human	Flowcytometry
Brilliant Violet 750™ anti-human CD185 (CXCR5)	J252D4	CD185	BioLegend	Human	Flowcytometry
Brilliant Violet 785™ anti-human CD49d	9F10	CD49d	BioLegend	Human	Flowcytometry
FITC anti-human CD57	HNK-1	CD57	BioLegend	Human	Flowcytometry
PE/Cyanine5 anti-human HLA-DR	L243	HLA-DR	BioLegend	Human	Flowcytometry
PE/Fire™ 700 anti-human CD25	M-A251	CD25	BioLegend	Human	Flowcytometry
PerCP/Cyanine5.5 anti-human CD27	M-T271	CD27	BioLegend	Human	Flowcytometry
Alexa Fluor® 700 anti-human CD127 (IL-7Rα)	A019D5	CD127	BioLegend	Human	Flowcytometry
APC/Fire™ 810 anti-human CD38	HIT2	CD38	BioLegend	Human	Flowcytometry
BD OptiBuild™ BUV395 Mouse Anti-Human CD45RA	5H9	CD45RA	BD Biosciences	Human	Flowcytometry

BD Horizon™ BUV496 Mouse Anti-Human CD16	3G8	CD16	BD Biosciences	Human	Flowcytometry
BD Horizon™ BUV737 Mouse Anti-Human CD56	NCAM16.2	CD56	BD Biosciences	Human	Flowcytometry
BD Horizon™ BUV805 Mouse Anti-Human CD8	SK1	CD8	BD Biosciences	Human	Flowcytometry
Brilliant Violet 510™ anti-human CD3	OKT3	CD3	BioLegend	Human	Flowcytometry
Pacific Blue™ anti-human CD161	HP-3G10	CD161	BioLegend	Human	Flowcytometry
PE anti-human TIGIT (VSTM3)	A15153G	TIGIT	BioLegend	Human	Flowcytometry
PE/Cyanine7 anti-human CD279 (PD-1)	EH12.2H7	CD279	BioLegend	Human	Flowcytometry
Spark Blue™ 550 anti-human CD4	SK3	CD4	BioLegend	Human	Flowcytometry
APC/Fire™ 750 anti-human/mouse Granzyme B	QA16A02	Granzyme B	BioLegend	Human	Flowcytometry
Brilliant Violet 605™ anti-human HLA-DR	L243	HLA-DR	BioLegend	Human	Flowcytometry
Brilliant Violet 650™ anti-human CD28	CD28.2	CD28	BioLegend	Human	Flowcytometry
Brilliant Violet 711™ anti-human CD39	A1	CD39	BioLegend	Human	Flowcytometry
BD OptiBuild™ BV750 Mouse Anti-Human TCR Vα7.2	OF-5A12	TCR Vα7.2	BD Biosciences	Human	Flowcytometry
Brilliant Violet 785™ anti-human CD27	O323	CD27	BioLegend	Human	Flowcytometry
BD Horizon™ PE-CF594 Mouse Anti-EOMES	X4-83	EOMES	BD Biosciences	Human	Flowcytometry
PerCP/Cyanine5.5 anti-human Granzyme A	CB9	Granzyme A	BioLegend	Human	Flowcytometry
Spark NIR™ 685 anti-human FOXP3	206D	FOXP3	BioLegend	Human	Flowcytometry
Anti-Hu CD20-BX007—Alexa Fluor™ 750	L26	CD20	Akoya	Human	Phenocycler
Anti-Hu CD31-BX001—Alexa Fluor™ 750	EP3095	CD31	Akoya	Human	Phenocycler
Anti-Hu Pan-Cytokeratin-BX019—Alexa Fluor™ 750	AE1-AE3	PANCK	Akoya	Human	Phenocycler
Anti-Hu CD8-BX026—Atto 550	C8/144B	CD8	Akoya	Human	Phenocycler
Anti-Hu CD21-BX032—Atto 550	EP3093	CD21	Akoya	Human	Phenocycler
Anti-Hu CD38-BX089—Atto 550	*AKYP0110**	CD38	Akoya	Human	Phenocycler
Anti-Hu IFNG-BX020—Atto 550	*AKYP0093**	IFNG	Akoya	Human	Phenocycler
Anti-Hu PD-1-BX046—Cy5	NAT105	CD279	Akoya	Human	Phenocycler
Anti-Hu ICOS-BX054—Cy5	SP98	ICOS	Akoya	Human	Phenocycler
Anti-Hu CD4-BX003—Cy5	EPR6855	CD4	Akoya	Human	Phenocycler
Anti-Hu CD3-BX045—Cy5	EP449E	CD3	Akoya	Human	Phenocycler
Anti-Hu CXCR5-BX042—Cy5	EPR23463-30	CXCR5	Abcam	Human	Phenocycler
PerCP/Cyanine5.5 anti-mouse CD4	RM4-5	CD4	BD Biosciences	Mouse	Flowcytometry

FITC anti-mouse CD4	GK1.5	CD4	BioLegend	Mouse	Flowcytometry
FITC anti-mouse CD8a	53-6.7	CD8	BD Biosciences	Mouse	Flowcytometry
APC anti-mouse CD44	IM7	CD44	BioLegend	Mouse	Flowcytometry
APC/Cyanine7 anti-mouse CD44	IM7	CD44	BioLegend	Mouse	Flowcytometry
Brilliant Violet 421™ anti-mouse CD279 (PD-1)	J43	CD279	BioLegend	Mouse	Flowcytometry
APC anti-mouse TIGIT	4D4	TIGIT	BioLegend	Mouse	Flowcytometry
Brilliant Violet 510™ anti-mouse CD19	1D3	CD19	BioLegend	Mouse	Flowcytometry

879 **Akoya references*

880 **Supplementary Table1.** Antibody listing

881 **Acknowledgements**

882 We thank the biological resource centre for biobanking (CHU Nantes, Hôtel Dieu, Centre de ressources
883 biologiques (CRB), Nantes, F-44093, France (BRIF : BB-0033-00040)). We thanks all the member of the
884 HEPATIMGO network. We thank the BIRD Core facility of the SFR Santé F. Bonamy (Université de
885 Nantes, Inserm UMS016, CNRS UMS3556). We thank the Genomics core facility and the Computational
886 Biology, Biostatistics and Modeling (CB2M) hub of CIML. Centre de Calcul Intensif d'Aix-Marseille is
887 acknowledged for granting access to its high performance computing resources. Supported by the
888 "Agence Nationale de la Recherche" (ANR-19-CE17-0024), the patient association "Association pour la
889 lutte contre les maladies inflammatoires du foie et des voies biliaires" (ALBI), the "Fondation Maladies
890 Rares" (including the « High throughput sequencing and rare diseases » program), the "Région pays de
891 la loire", the LabEx IGO program (n° ANR-11-LABX-0016) funded by the «Investment into the Future»
892 French Government program managed by the "Agence Nationale de la Recherche" (ANR). This work
893 was supported by institutional grants from INSERM, CNRS and Aix-Marseille University to the CIML.

894 **Author Contributions**

895 A. C. and T. G. performed the experiments, analyzed the data and wrote the manuscript; C. D. analyzed
896 the data; L. G and S. A. performed the experiments, P-J. G. performed the experiments and analyzed
897 the data; M. B. analyzed the data; R. D. analyzed the data; C. S. performed the experiments and
898 analyzed the data; A. D. performed the experiments; P. P-G. supervised data analysis, analyzed the
899 data and wrote the manuscript; C. C. managed human AILD samples collection and patient data base;
900 L. B. and J-P. J. performed experiments; C. F. performed experiments; A. I., M. K., E. B-J., L. E. A. L., C.
901 S., M. S. and F. T. provided human AILD samples and critical insight in AILD pathology; F. V. managed
902 human AILD samples collection; L. B. performed the experiments; S. B. provided critical insight the
903 study design, W. W. K. provided the MHC class II tetramer technology; J-F. M. provided human liver

904 AILD biopsies and critical insight in histology analysis; A. L. provided human AILD samples and critical
905 insight in AILD pathology; J. P. supervised data analysis; M. B. supervised data analysis and critical
906 insight TCR sequencing; J. G. provided human AILD samples, critical insight in AILD pathology and
907 direction in the study design; S. C. designed the study, supervised data analysis and wrote the
908 manuscript; P. M. designed the study, supervised data analysis and wrote the manuscript, A. R.
909 designed the study, supervised data analysis, performed the experiments, analyzed the data and wrote
910 the manuscript. All authors reviewed and approved the manuscript.

911 **Conflicts of Interest**

912 The authors declare no conflict of interest related to this work.

913 **Data Availability**

914 Single-cell RNA sequencing raw data from the different experiments analyzed in this article have been
915 deposited in the NCBI GEO repository under accession numbers XXXXX. Processed and annotated
916 single-cell RNA-sequencing datasets analyzed in this article are available in the following repository:
917 XXXXX. Scripts used for analyzing the datasets and produce the figures of this article are available in
918 the following repository: GitHub/XXXX.

919 **References:**

920 1. Poch, T., Krause, J., Casar, C., Liwinski, T., Glau, L., Kaufmann, M., Ahrenstorf, A.E., Hess, L.U.,
921 Ziegler, A.E., Martrus, G., et al. (2021). Single-cell atlas of hepatic T cells reveals expansion of liver-
922 resident naive-like CD4+ T cells in primary sclerosing cholangitis. Journal of Hepatology *75*, 414–423.
923 10.1016/j.jhep.2021.03.016.

924 2. Zimmer, C.L., Von Seth, E., Buggert, M., Strauss, O., Hertwig, L., Nguyen, S., Wong, A.Y.W.,
925 Zotter, C., Berglin, L., Michaëlsson, J., et al. (2021). A biliary immune landscape map of primary
926 sclerosing cholangitis reveals a dominant network of neutrophils and tissue-resident T cells. Sci.
927 Transl. Med. *13*, eabb3107. 10.1126/scitranslmed.abb3107.

928 3. Andrews, T.S., Nakib, D., Perciani, C.T., Ma, X.Z., Liu, L., Winter, E., Camat, D., Chung, S.W.,
929 Lumanto, P., Manuel, J., et al. (2024). Single-cell, single-nucleus, and spatial transcriptomics
930 characterization of the immunological landscape in the healthy and PSC human liver. Journal of
931 Hepatology, S0168827824000035. 10.1016/j.jhep.2023.12.023.

932 4. Webb, G.J., Hirschfield, G.M., Krawitt, E.L., and Gershwin, M.E. (2018). Cellular and Molecular
933 Mechanisms of Autoimmune Hepatitis. Annu. Rev. Pathol. Mech. Dis. *13*, 247–292. 10.1146/annurev-
934 pathol-020117-043534.

935 5. European Association for the Study of the Liver (2015). EASL Clinical Practice Guidelines:
936 Autoimmune hepatitis. J. Hepatol. *63*, 971–1004. 10.1016/j.jhep.2015.06.030.

937 6. Bowlus, C.L., and Gershwin, M.E. (2014). The diagnosis of primary biliary cirrhosis.
938 Autoimmunity Reviews *13*, 441–444. 10.1016/j.autrev.2014.01.041.

939 7. European Association for the Study of the Liver. Electronic address: easloffice@easloffice.eu
940 and European Association for the Study of the Liver (2017). EASL Clinical Practice Guidelines: The
941 diagnosis and management of patients with primary biliary cholangitis. J. Hepatol. *67*, 145–172.
942 10.1016/j.jhep.2017.03.022.

943 8. Sirpal, S., and Chandok, N. (2017). Primary sclerosing cholangitis: diagnostic and management
944 challenges. Clin Exp Gastroenterol *10*, 265–273. 10.2147/CEG.S105872.

945 9. You, Z., Li, Y., Wang, Q., Zhao, Z., Li, Y., Qian, Q., Li, B., Zhang, J., Huang, B., Liang, J., et al.
946 (2021). The Clinical Significance of Hepatic $CD69^+CD103^+CD8^+$ Resident-Memory T Cells in
947 Autoimmune Hepatitis. Hepatology *74*, 847–863. 10.1002/hep.31739.

948 10. Ellinghaus, D. (2022). How genetic risk contributes to autoimmune liver disease. Semin
949 Immunopathol *44*, 397–410. 10.1007/s00281-022-00950-8.

950 11. Chen, H., Han, Z., Fan, Y., Chen, L., Peng, F., Cheng, X., Wang, Y., Su, J., and Li, D. (2023). CD4+
951 T-cell subsets in autoimmune hepatitis: A review. Hepatology Communications *7*.
952 10.1097/HC9.0000000000000269.

953 12. Cardon, A., Conchon, S., and Renand, A. (2021). Mechanisms of autoimmune hepatitis. Curr
954 Opin Gastroenterol *37*, 79–85. 10.1097/MOG.0000000000000704.

955 13. Than, N.N., Hodson, J., Schmidt-Martin, D., Taubert, R., Wawman, R.E., Botter, M., Gautam,
956 N., Bock, K., Jones, R., Appanna, G.D., et al. (2019). Efficacy of rituximab in difficult-to-manage
957 autoimmune hepatitis: Results from the International Autoimmune Hepatitis Group. JHEP Reports *1*,
958 437–445. 10.1016/j.jhepr.2019.10.005.

959 14. Longhi, M.S., Hussain, M.J., Bogdanos, D.P., Quaglia, A., Mieli-Vergani, G., Ma, Y., and
960 Vergani, D. (2007). Cytochrome P450IID6-specific CD8 T cell immune responses mirror disease
961 activity in autoimmune hepatitis type 2. Hepatology *46*, 472–484. 10.1002/hep.21658.

962 15. Löhr, H.F., Schlaak, J.F., Lohse, A.W., Böcher, W.O., Arenz, M., Gerken, G., and Meyer Zum
963 Büschenfelde, K.H. (1996). Autoreactive CD4+ LKM-specific and anticlonotypic T-cell responses in
964 LKM-1 antibody-positive autoimmune hepatitis. Hepatology *24*, 1416–1421.
965 10.1002/hep.510240619.

966 16. Chow, I.-T., James, E.A., Gates, T.J., Tan, V., Moustakas, A.K., Papadopoulos, G.K., and Kwok,
967 W.W. (2013). Differential Binding of Pyruvate Dehydrogenase Complex-E2 Epitopes by DRB1*08:01
968 and DRB1*11:01 Is Predicted by Their Structural Motifs and Correlates with Disease Risk. The Journal
969 of Immunology *190*, 4516–4524. 10.4049/jimmunol.1202445.

970 17. Mix, H., Weiler-Normann, C., Thimme, R., Ahlenstiel, G., Shin, E.-C., Herkel, J., David, C.S.,
971 Lohse, A.W., and Rehermann, B. (2008). Identification of CD4 T-cell epitopes in soluble liver
972 antigen/liver pancreas autoantigen in autoimmune hepatitis. Gastroenterology *135*, 2107–2118.
973 10.1053/j.gastro.2008.07.029.

974 18. Ehser, J., Holdener, M., Christen, S., Bayer, M., Pfeilschifter, J.M., Hintermann, E., Bogdanos,
975 D., and Christen, U. (2013). Molecular mimicry rather than identity breaks T-cell tolerance in the
976 CYP2D6 mouse model for human autoimmune hepatitis. J. Autoimmun. *42*, 39–49.
977 10.1016/j.jaut.2012.11.001.

978 19. Hardtke-Wolenski, M., Fischer, K., Noyan, F., Schlue, J., Falk, C.S., Stahlhut, M., Woller, N.,
979 Kuehnel, F., Taubert, R., Manns, M.P., et al. (2013). Genetic predisposition and environmental danger

980 signals initiate chronic autoimmune hepatitis driven by CD4+ T cells. Hepatology *58*, 718–728.
981 10.1002/hep.26380.

982 20. Holdener, M., Hintermann, E., Bayer, M., Rhode, A., Rodrigo, E., Hintereder, G., Johnson, E.F.,
983 Gonzalez, F.J., Pfeilschifter, J., Manns, M.P., et al. (2008). Breaking tolerance to the natural human
984 liver autoantigen cytochrome P450 2D6 by virus infection. J. Exp. Med. *205*, 1409–1422.
985 10.1084/jem.20071859.

986 21. Lapierre, P., Djilali-Saiah, I., Vitozzi, S., and Alvarez, F. (2004). A murine model of type 2
987 autoimmune hepatitis: Xenoimmunization with human antigens. Hepatology *39*, 1066–1074.
988 10.1002/hep.20109.

989 22. Renand, A., Cervera-Marzal, I., Gil, L., Dong, C., Garcia, A., Kervagoret, E., Aublé, H., Habes, S.,
990 Chevalier, C., Vavasseur, F., et al. (2020). Integrative molecular profiling of autoreactive CD4 T cells in
991 autoimmune hepatitis. Journal of Hepatology *73*, 1379–1390. 10.1016/j.jhep.2020.05.053.

992 23. Rao, D.A., Gurish, M.F., Marshall, J.L., Slowikowski, K., Fonseka, C.Y., Liu, Y., Donlin, L.T.,
993 Henderson, L.A., Wei, K., Mizoguchi, F., et al. (2017). Pathologically expanded peripheral T helper cell
994 subset drives B cells in rheumatoid arthritis. Nature *542*, 110–114. 10.1038/nature20810.

995 24. Zhang, F., Wei, K., Slowikowski, K., Fonseka, C.Y., Rao, D.A., Kelly, S., Goodman, S.M.,
996 Tabechian, D., Hughes, L.B., Salomon-Escoto, K., et al. (2019). Defining inflammatory cell states in
997 rheumatoid arthritis joint synovial tissues by integrating single-cell transcriptomics and mass
998 cytometry. Nat. Immunol. *20*, 928–942. 10.1038/s41590-019-0378-1.

999 25. Marks, K.E., and Rao, D.A. (2022). T peripheral helper cells in autoimmune diseases*.
1000 Immunological Reviews *307*, 191–202. 10.1111/imr.13069.

1001 26. Arazi, A., Rao, D.A., Berthier, C.C., Davidson, A., Liu, Y., Hoover, P.J., Chicoine, A., Eisenhaure,
1002 T.M., Jonsson, A.H., Li, S., et al. (2019). The immune cell landscape in kidneys of patients with lupus
1003 nephritis. Nat. Immunol. *20*, 902–914. 10.1038/s41590-019-0398-x.

1004 27. Han, D., Lee, A.Y., Kim, T., Choi, J.Y., Cho, M.Y., Song, A., Kim, C., Shim, J.H., Kim, H.J., Kim, H.,
1005 et al. (2023). Microenvironmental network of clonal CXCL13+CD4+ T cells and Tregs in pemphigus
1006 chronic blisters. Journal of Clinical Investigation *133*, e166357. 10.1172/JCI166357.

1007 28. Harada, T., Kikushige, Y., Miyamoto, T., Uno, K., Niiro, H., Kawakami, A., Koga, T., Akashi, K.,
1008 and Yoshizaki, K. (2023). Peripheral helper-T-cell-derived CXCL13 is a crucial pathogenic factor in
1009 idiopathic multicentric Castleman disease. Nat Commun *14*, 6959. 10.1038/s41467-023-42718-0.

1010 29. Christophersen, A., Lund, E.G., Snir, O., Solà, E., Kanduri, C., Dahal-Koirala, S., Zühlke, S.,
1011 Molberg, Ø., Utz, P.J., Rohani-Pichavant, M., et al. (2019). Distinct phenotype of CD4+ T cells driving
1012 celiac disease identified in multiple autoimmune conditions. Nat. Med. *25*, 734–737.
1013 10.1038/s41591-019-0403-9.

1014 30. Yong, L., Chunyan, W., Yan, Y., Wanyu, L., Huifan, J., Pingwei, Z., and Yanfang, J. (2021).
1015 Expanded circulating peripheral helper T cells in primary biliary cholangitis. Molecular Immunology
1016 *131*, 44–50. 10.1016/j.molimm.2020.09.007.

1017 31. Kita, H., Matsumura, S., He, X.-S., Ansari, A.A., Lian, Z.-X., Van de Water, J., Coppel, R.L.,
1018 Kaplan, M.M., and Gershwin, M.E. (2002). Quantitative and functional analysis of PDC-E2–specific
1019 autoreactive cytotoxic T lymphocytes in primary biliary cirrhosis. J. Clin. Invest. *109*, 1231–1240.
1020 10.1172/JCI0214698.

1021 32. Van de Water, J., Ansari, A., Prindiville, T., Coppel, R.L., Ricalton, N., Kotzin, B.L., Liu, S.,
1022 Roche, T.E., Krams, S.M., Munoz, S., et al. (1995). Heterogeneity of autoreactive T cell clones specific
1023 for the E2 component of the pyruvate dehydrogenase complex in primary biliary cirrhosis. J Exp Med
1024 *181*, 723–733. 10.1084/jem.181.2.723.

1025 33. Shimoda, S., Ishikawa, F., Kamihira, T., Komori, A., Niiro, H., Baba, E., Harada, K., Isse, K.,
1026 Nakanuma, Y., Ishibashi, H., et al. (2006). Autoreactive T-Cell Responses in Primary Biliary Cirrhosis
1027 Are Proinflammatory Whereas Those of Controls Are Regulatory. Gastroenterology *131*, 606–618.
1028 10.1053/j.gastro.2006.05.056.

1029 34. Bovensiepen, C.S., Schakat, M., Sebode, M., Zenouzi, R., Hartl, J., Peiseler, M., Li, J., Henze, L.,
1030 Woestemeier, A., Schramm, C., et al. (2019). TNF-Producing Th1 Cells Are Selectively Expanded in
1031 Liver Infiltrates of Patients with Autoimmune Hepatitis. J. Immunol. *203*, 3148–3156.
1032 10.4049/jimmunol.1900124.

1033 35. Nguyen, Q.P., Takehara, K.K., Deng, T.Z., O'Shea, S., Heeg, M., Omilusik, K.D., Milner, J.J.,
1034 Quon, S., Pipkin, M.E., Choi, J., et al. (2023). Transcriptional programming of $CD4^+ T_{RM}$ differentiation
1035 in viral infection balances effector- and memory-associated gene expression. Sci. Immunol. *8*,
1036 eabq7486. 10.1126/sciimmunol.abq7486.

1037 36. Poon, M.M.L., Caron, D.P., Wang, Z., Wells, S.B., Chen, D., Meng, W., Szabo, P.A., Lam, N.,
1038 Kubota, M., Matsumoto, R., et al. (2023). Tissue adaptation and clonal segregation of human memory
1039 T cells in barrier sites. Nat Immunol *24*, 309–319. 10.1038/s41590-022-01395-9.

1040 37. Yossef, R., Krishna, S., Sindiri, S., Lowery, F.J., Copeland, A.R., Gartner, J.J., Parkhurst, M.R.,
1041 Parikh, N.B., Hitscherich, K.J., Levi, S.T., et al. (2023). Phenotypic signatures of circulating neoantigen-
1042 reactive CD8+ T cells in patients with metastatic cancers. Cancer Cell *41*, 2154-2165.e5.
1043 10.1016/j.ccell.2023.11.005.

1044 38. Bocharnikov, A.V., Keegan, J., Wacleche, V.S., Cao, Y., Fonseka, C.Y., Wang, G., Muise, E.S.,
1045 Zhang, K.X., Arazi, A., Keras, G., et al. (2019). PD-1hiCXCR5- T peripheral helper cells promote B cell
1046 responses in lupus via MAF and IL-21. JCI Insight *4*. 10.1172/jci.insight.130062.

1047 39. Argyriou, A., Wadsworth, M.H., Lendvai, A., Christensen, S.M., Hensvold, A.H., Gerstner, C.,
1048 Van Vollenhoven, A., Kravarik, K., Winkler, A., Malmström, V., et al. (2022). Single cell sequencing
1049 identifies clonally expanded synovial CD4+ TPH cells expressing GPR56 in rheumatoid arthritis. Nat
1050 Commun *13*, 4046. 10.1038/s41467-022-31519-6.

1051 40. Lowery, F.J., Krishna, S., Yossef, R., Parikh, N.B., Chatani, P.D., Zacharakis, N., Parkhurst, M.R.,
1052 Levin, N., Sindiri, S., Sachs, A., et al. (2022). Molecular signatures of antitumor neoantigen-reactive T
1053 cells from metastatic human cancers. Science *375*, 877–884. 10.1126/science.abl5447.

1054 41. Balança, C.-C., Salvioni, A., Scarlata, C.-M., Michelas, M., Martinez-Gomez, C., Gomez-Roca,
1055 C., Sarradin, V., Tosolini, M., Valle, C., Pont, F., et al. (2021). PD-1 blockade restores helper activity of
1056 tumor-infiltrating, exhausted PD-1hiCD39+ CD4 T cells. JCI Insight *6*, e142513.
1057 10.1172/jci.insight.142513.

1058 42. Duhen, R., Fesneau, O., Samson, K.A., Frye, A.K., Beymer, M., Rajamanickam, V., Ross, D.,
1059 Tran, E., Bernard, B., Weinberg, A.D., et al. (2022). PD-1 and ICOS coexpression identifies tumor-
1060 reactive CD4+ T cells in human solid tumors. Journal of Clinical Investigation *132*, e156821.
1061 10.1172/JCI156821.

1062 43. Magen, A., Hamon, P., Fiaschi, N., Soong, B.Y., Park, M.D., Mattiuz, R., Humblin, E., Troncoso,
1063 L., D'souza, D., Dawson, T., et al. (2023). Intratumoral dendritic cell–CD4+ T helper cell niches enable
1064 CD8+ T cell differentiation following PD-1 blockade in hepatocellular carcinoma. Nat Med *29*, 1389–
1065 1399. 10.1038/s41591-023-02345-0.

1066 44. Zhang, C., Li, J., Cheng, Y., Meng, F., Song, J.-W., Fan, X., Fan, H., Li, J., Fu, Y.-L., Zhou, M.-J., et
1067 al. (2023). Single-cell RNA sequencing reveals intrahepatic and peripheral immune characteristics
1068 related to disease phases in HBV-infected patients. Gut *72*, 153–167. 10.1136/gutjnl-2021-325915.

1069 45. Wiggins, B.G., Pallett, L.J., Li, X., Davies, S.P., Amin, O.E., Gill, U.S., Kucykowicz, S., Patel, A.M.,
1070 Aliazis, K., Liu, Y.S., et al. (2022). The human liver microenvironment shapes the homing and function
1071 of $CD4^+$ T-cell populations. Gut *71*, 1399–1411. 10.1136/gutjnl-2020-323771.

1072 46. Hanada, K., Zhao, C., Gil-Hoyos, R., Gartner, J.J., Chow-Parmer, C., Lowery, F.J., Krishna, S.,
1073 Prickett, T.D., Kivitz, S., Parkhurst, M.R., et al. (2022). A phenotypic signature that identifies
1074 neoantigen-reactive T cells in fresh human lung cancers. Cancer Cell *40*, 479-493.e6.
1075 10.1016/j.ccell.2022.03.012.

1076 47. De Martin, E., Michot, J.-M., Papouin, B., Champiat, S., Mateus, C., Lambotte, O., Roche, B.,
1077 Antonini, T.M., Coilly, A., Laghouati, S., et al. (2018). Characterization of liver injury induced by cancer
1078 immunotherapy using immune checkpoint inhibitors. J. Hepatol. *68*, 1181–1190.
1079 10.1016/j.jhep.2018.01.033.

1080 48. Zen, Y., and Yeh, M.M. (2018). Hepatotoxicity of immune checkpoint inhibitors: a histology
1081 study of seven cases in comparison with autoimmune hepatitis and idiosyncratic drug-induced liver
1082 injury. Modern Pathology *31*, 965–973. 10.1038/s41379-018-0013-y.

1083 49. Hagiwara, S., Watanabe, T., Kudo, M., Minaga, K., Komeda, Y., Kamata, K., Kimura, M.,
1084 Hayashi, H., Nakagawa, K., Ueshima, K., et al. (2021). Clinicopathological analysis of hepatic immune-
1085 related adverse events in comparison with autoimmune hepatitis and graft-versus host disease. Sci
1086 Rep *11*, 9242. 10.1038/s41598-021-88824-1.

1087 50. Li, Y., Sun, Y., Liu, Y., Wang, B., Li, J., Wang, H., Zhang, H., Wang, X., Han, X., Lin, Q., et al.
1088 (2022). Genome-wide meta-analysis identifies susceptibility loci for autoimmune hepatitis type 1.
1089 Hepatology *76*, 564–575. 10.1002/hep.32417.

1090 51. Agarwal, K., Czaja, A.J., Jones, D.E., and Donaldson, P.T. (2000). Cytotoxic T lymphocyte
1091 antigen-4 (CTLA-4) gene polymorphisms and susceptibility to type 1 autoimmune hepatitis.
1092 Hepatology *31*, 49–53. 10.1002/hep.510310110.

1093 52. Agarwal, K., Jones, D.E., Daly, A.K., James, O.F., Vaidya, B., Pearce, S., and Bassendine, M.F.
1094 (2000). CTLA-4 gene polymorphism confers susceptibility to primary biliary cirrhosis. J Hepatol *32*,
1095 538–541. 10.1016/s0168-8278(00)80213-5.

1096 53. Juran, B.D., Atkinson, E.J., Schlicht, E.M., Fridley, B.L., Petersen, G.M., and Lazaridis, K.N.
1097 (2007). Interacting alleles of the coinhibitory immunoreceptor genes cytotoxic T-lymphocyte antigen
1098 4 and programmed cell-death 1 influence risk and features of primary biliary cirrhosis. Hepatology
1099 *47*, 563–570. 10.1002/hep.22048.

1100 54. Joshita, S., Umemura, T., Yoshizawa, K., Katsuyama, Y., Tanaka, E., Nakamura, M., Ishibashi,
1101 H., Ota, M., and Shinshu PBC Study Group (2010). Association analysis of cytotoxic T-lymphocyte
1102 antigen 4 gene polymorphisms with primary biliary cirrhosis in Japanese patients. J Hepatol *53*, 537–
1103 541. 10.1016/j.jhep.2010.03.017.

1104 55. Qin, B., Li, J., Liang, Y., Yang, Z., and Zhong, R. (2014). The association between Cytotoxic T
1105 Lymphocyte Associated Antigen-4, Fas, Tumour Necrosis Factor-α gene polymorphisms and
1106 autoimmune hepatitis: A meta-analysis. Digestive and Liver Disease *46*, 541–548.
1107 10.1016/j.dld.2014.02.003.

1108 56. Hennes, E.M., Zeniya, M., Czaja, A.J., Parés, A., Dalekos, G.N., Krawitt, E.L., Bittencourt, P.L.,
1109 Porta, G., Boberg, K.M., Hofer, H., et al. (2008). Simplified criteria for the diagnosis of autoimmune
1110 hepatitis. Hepatology *48*, 169–176. 10.1002/hep.22322.

1111 57. Renand, A., Habes, S., Mosnier, J.-F., Aublé, H., Judor, J.-P., Vince, N., Hulin, P., Nedellec, S.,
1112 Métairie, S., Archambeaud, I., et al. (2018). Immune Alterations in Patients With Type 1 Autoimmune
1113 Hepatitis Persist Upon Standard Immunosuppressive Treatment. Hepatol Commun *2*, 968–981.
1114 10.1002/hep4.1202.

1115 58. Attaf, N., Cervera-Marzal, I., Dong, C., Gil, L., Renand, A., Spinelli, L., and Milpied, P. (2020).
1116 FB5P-seq: FACS-Based 5-Prime End Single-Cell RNA-seq for Integrative Analysis of Transcriptome and
1117 Antigen Receptor Repertoire in B and T Cells. Front. Immunol. *11*, 216. 10.3389/fimmu.2020.00216.

1118 59. Hahaut, V., Pavlinic, D., Carbone, W., Schuierer, S., Balmer, P., Quinodoz, M., Renner, M.,
1119 Roma, G., Cowan, C.S., and Picelli, S. (2022). Fast and highly sensitive full-length single-cell RNA
1120 sequencing using FLASH-seq. Nat Biotechnol *40*, 1447–1451. 10.1038/s41587-022-01312-3.

1121 60. Parekh, S., Ziegenhain, C., Vieth, B., Enard, W., and Hellmann, I. (2018). zUMIs - A fast and
1122 flexible pipeline to process RNA sequencing data with UMIs. GigaScience *7*.
1123 10.1093/gigascience/giy059.

1124 61. Song, L., Cohen, D., Ouyang, Z., Cao, Y., Hu, X., and Liu, X.S. (2021). TRUST4: immune
1125 repertoire reconstruction from bulk and single-cell RNA-seq data. Nat Methods *18*, 627–630.
1126 10.1038/s41592-021-01142-2.

1127 62. Hao, Y., Hao, S., Andersen-Nissen, E., Mauck, W.M., Zheng, S., Butler, A., Lee, M.J., Wilk, A.J.,
1128 Darby, C., Zager, M., et al. (2021). Integrated analysis of multimodal single-cell data. Cell *184*, 3573-
1129 3587.e29. 10.1016/j.cell.2021.04.048.

1130 63. Korsunsky, I., Millard, N., Fan, J., Slowikowski, K., Zhang, F., Wei, K., Baglaenko, Y., Brenner,
1131 M., Loh, P., and Raychaudhuri, S. (2019). Fast, sensitive and accurate integration of single-cell data
1132 with Harmony. Nat Methods *16*, 1289–1296. 10.1038/s41592-019-0619-0.

1133 64. Schultheiß, C., Simnica, D., Willscher, E., Oberle, A., Fanchi, L., Bonzanni, N., Wildner, N.H.,
1134 Schulze Zur Wiesch, J., Weiler-Normann, C., Lohse, A.W., et al. (2020). Next-Generation
1135 Immunosequencing Reveals Pathological T-Cell Architecture in Autoimmune Hepatitis. Hepatology.
1136 10.1002/hep.31473.

1137 65. Tannour-Louet, M., Porteu, A., Vaulont, S., Kahn, A., and Vasseur-Cognet, M. (2002). A
1138 tamoxifen-inducible chimeric Cre recombinase specifically effective in the fetal and adult mouse
1139 liver. Hepatology *35*, 1072–1081. 10.1053/jhep.2002.33164.

1140 66. Saxena, A., Bauer, J., Scheikl, T., Zappulla, J., Audebert, M., Desbois, S., Waisman, A.,
1141 Lassmann, H., Liblau, R.S., and Mars, L.T. (2008). Cutting edge: Multiple sclerosis-like lesions induced
1142 by effector CD8 T cells recognizing a sequestered antigen on oligodendrocytes. J. Immunol. *181*,
1143 1617–1621.

1144 67. Le Guen, V., Judor, J.-P., Boeffard, F., Gauttier, V., Ferry, N., Soulillou, J.-P., Brouard, S., and
1145 Conchon, S. (2016). Alloantigen gene transfer to hepatocytes promotes tolerance to pancreatic islet
1146 graft by inducing CD8+ regulatory T cells. J. Hepatol. 10.1016/j.jhep.2016.11.019.

1147 68. Ishak, K., Baptista, A., Bianchi, L., Callea, F., De Groote, J., Gudat, F., Denk, H., Desmet, V.,
1148 Korb, G., and MacSween, R.N. (1995). Histological grading and staging of chronic hepatitis. J. Hepatol.
1149 *22*, 696–699.

1150 69. Danger, R., Moiteaux, Q., Feseha, Y., Geffard, E., Ramstein, G., and Brouard, S. (2021). FaDA:
1151 A web application for regular laboratory data analyses. PLoS One *16*, e0261083.
1152 10.1371/journal.pone.0261083.

1153